Assessment of Spatiotemporal Characteristic of Droughts Using *In Situ* and Remote Sensing-Based Drought Indices

Sepideh Jalayer, Alireza Sharifi, Dariush Abbasi-Moghadam, Aqil Tariq, and Shujing Qin

***Abstract*—Drought has been identified as one of the significant complicated natural disasters exacerbated by land degradation and climate change. Hence, monitoring drought and evaluating its spatiotemporal dynamics are essential to manage regional drought conditions and protecting the natural environment. In this study, various single remote sensing-based drought indices including soil moisture condition index (SMCI), precipitation condition index (PCI), temperature condition index (TCI), and vegetation condition index (VCI) and combined RS-based drought Indices including optimized meteorological drought index (OMDI) and synthesized drought index (SDI) have been used to investigate the spatiotemporal variations of meteorological and agricultural droughts between 2000 and 2021 in Iran. The *in situ* drought indices, including the standardized precipitation index (SPI) and standardized precipitation evapotranspiration index (SPEI) series of 1, 3, 6, 12, and 24 months were utilized to verify remote sensing-based drought indices and evaluate their applicability for analyzing drought conditions. The results indicated that the correlation coefficients of the *in situ* drought indices with the combined drought indices are higher than the RS-based single drought indexes. Generally, single-factor drought indexes, including VCI, TCI, PCI, and SMCI, have specific characteristics. The PCI and SMCI have an acceptable correlation with the short-term SPI and SPEI and are more applicable to monitoring short-term drought conditions. Further, the TCI has better performance in monitoring long-term drought conditions in Iran. This research concluded that the central, eastern, and southeastern parts of Iran mainly were experiencing exceptional and extreme drought conditions as the worst agricultural and meteorological drought conditions observed in the years 2008 and 2021 in the region during the last 20 years. The results also showed that, in 2019 and 2020, most areas of Iran had higher OMDI and SDI values and the severity of the drought has decreased in these years. Particularly, this research provides an essential reference for reasonably choosing RS-based drought indices for monitoring meteorological and agricultural droughts from a local to global scale.**

***Index Terms*—Agricultural drought, combined drought index, optimized meteorological drought index (OMDI), standardized precipitation evapotranspiration index (SPEI), synthesized drought index (SDI).**

Manuscript received 1 September 2022; revised 13 November 2022 and 12 December 2022; accepted 13 January 2023. Date of publication 16 January 2023; date of current version 27 January 2023. This work was supported in part by the National Natural Science Foundation of China under Grant 52209068 and in part by the Postdoctoral Research Foundation of China under Grant 2020M682477. *(Corresponding authors: Aqil Tariq; Shujing Qin.)*

Sepideh Jalayer and Alireza Sharifi are with the Faculty of Civil Engineering, Shahid Rajaee Teacher Training University, Tehran 16785-163, Iran (e-mail: sepideh.jal@gmail.com; a_sharifi@sru.ac.ir).

Dariush Abbasi-Moghadam is with the Department of Electrical Engineering, Shahid Bahonar University of Kerman, Kerman 76169-14111, Iran (e-mail: abbasimoghadam@uk.ac.ir).

Aqil Tariq is with the State Key Laboratory of Information Engineering in Surveying Mapping and Remote Sensing, Wuhan University, Wuhan 430079, China, and also with the Department of Wildlife, Fisheries and Aquaculture, College of Forest Resources, Mississippi State University, MS 39762-9690 USA (e-mail: aqiltariq@whu.edu.cn; at2139@msstate.edu).

Shujing Qin is with the State Key Laboratory of Water Resources and Hydropower Engineering Science, Wuhan University, Wuhan 430072, China (e-mail: shujing.qin@whu.edu.cn).

Digital Object Identifier 10.1109/JSTARS.2023.3237380

I. Introduction

DROUGHT is expressed as prolonged water scarcity, whether atmospheric (below-normal precipitation), or surface and subsurface water, which can last for months or years. Drought leads to soil retrogression and degradation, water scarcity, desertification, vegetation destruction, sandstorm, wildfire, and other disaster phenomena [1], [2], [3]. Drought ranks first among different types of hazards due to climate change [4]. Changes in rainfall patterns and temperature are the critical determinant elements of drought, causing significant losses to agriculture and affecting crop production [5], [6]. Therefore, monitoring and assessment of drought and analyzing its spatiotemporal dynamics on multiple time scales are essential to protect the natural environment, restore pastures and balance land and water resources against regional drought conditions [7]. One of the most manageable steps we can take to help mitigate the impacts of drought is sustainable water management as well as, using remote sensing datasets to assess drought-related variables and categorize drought severity across large regions. Drought is often grouped into four basic categories: meteorological, hydrological, agricultural, and socio-economic [8], [9], [10], [11]. Meteorological drought refers to the degree of dryness or lack of precipitation and the length of the dry period. Agricultural drought relates various meteorological drought characteristics to agricultural effects, focusing on deficiency in rainfall, differences between the actual (ET_a) and the potential evapotranspiration (PET), and lack of soil moisture (SM) [12]. Hydrological drought is defined as the lack of surface and underground water supplies. It is measurable by evaluating stream flow, snowpack, and lake and groundwater levels. To understand the association between agricultural and meteorological droughts, it is necessary to examine the correlation between vegetation indices and climate variability [5], [13], [14], [15], [16].

Traditional procedures for monitoring drought conditions are based on ground measurements of hydro-climatic variables, including rainfall, temperature, relative humidity, and soil water content. For instance, the palmer drought severity index (PDSI) utilizes rainfall and temperature, the standardized precipitation index (SPI) uses rainfall regimes, crop moisture index integrates SM, rainfall, and temperature, standardized anomaly index uses rainfall variability, and soil moisture drought index incorporates weekly SM and evapotranspiration values [17], [18], [19], [20], [21]. However, the number and uneven spatial distribution of available stations across the landscape impact the reliability of such interpolation. As well as, the implementation of the observation stations is often time-consuming, expensive, and can fail for many reasons. Therefore, remote sensing data, because of its continuous and comprehensive datasets from precipitation, temperature, SM, PET and ET_a, and vegetation growth, can be employed to analyze drought spatiality during a long period of time. RS datasets have been utilized to assess drought-related variables and categorize drought severity across large regions [22]. Satellite precipitation products (SPPs) are the most important sources of data for analyzing the spatial distribution of precipitation and seasonal drought monitoring. There are various SPPs available, such as the Climate Prediction Center morphing method, Tropical Rainfall Measuring Mission (TRMM), and Global Satellite Mapping of Precipitation to produce drought indices [23], [24], [25].

A number of distinct drought indices derived from RS-based datasets have been developed to exhibit drought conditions. Pei et al. [26] proposed the vegetation condition index (VCI) formed on the relative normalized difference vegetation index (NDVI) change considering the minimum historical NDVI value. The VCI has been evaluated to monitor water stress conditions and assess the intensity, duration, and effect of vegetation drought. Pei et al. also, by normalizing land surface temperature (LST) values to the maximum range of a particular area, developed the temperature condition index (TCI) to assess stress on vegetation as a consequence of temperatures and severe wetness. The TCI and VCI have been used to evaluate thermal conditions and cumulative humidity over a range of vegetation types and determine the spatiotemporal variations of drought across the world [27], [28]. The soil moisture condition index (SMCI) illustrates SM condition considering the historical values, and the SMCI value range changes between 0 and 100, where the value close to 0 indicates extreme SM stress, while values nearby 100 describe the extremely wet condition. The PCI is a meteorological drought index to evaluate the concentration and variability of rainfall in time, which ranges from 0 to 100 based on variations in rainfall from highly unfavorable to optimal [29], [30], [31], [32].

Different approaches have been employed to detect drought conditions for various underlying surfaces and monitor drought processes. Kloos et al. [33] applied the drought indexes, including TCI, VCI, and vegetation health index (VHI), and analyzed correlations between NDVI and LST from 2001 to 2020. Jiang et al. [34] utilized the Pearson correlation analysis to evaluate the relationships among climatic factors, vegetation conditions, and drought. In addition, they used a regression model to analyze the impacts of climatic factors on vegetation coverage based on the standardized evapotranspiration deficit index, NDVI, and gridded meteorological dataset in China [34]. Zeng et al. [6] evaluated the sc-PDSI and the standardized precipitation evapotranspiration index (SPEI) as drought indices to enhance the drought monitoring capability of VHI. Almeida-Ñauñay et al. [35] calculated meteorological drought indices, including SPI and SPEI, and agriculture drought indexes, including VHI and standardized VHI (SVHI), to optimize the correlation between both drought types. Pei et al. [36] analyzed NDVI–climate relationship at the 30-day time scale. They assessed temporal variations in NDVI and climate variables and discovered the correlation coefficient between them. Wang et al. evaluated the spatiotemporal variations of LST, NDVI, and the relationship between them was examined in China over a period of 16 years. In addition, eight scenarios have been determined to investigate the driving forces in vegetation dynamics [37]. All these studies have utilized single drought indices to detect meteorological and agricultural droughts and analyzed the correlation between both types of droughts.

Accordingly, in this research, combined drought indexes have been employed to investigate the spatiotemporal variations of meteorological and agricultural droughts and analyze the association between them. This study has been conducted to specify the spatiotemporal characteristics of meteorological drought on the annual scales over the period 2000–2021 in a large study area using the optimized meteorological drought index (OMDI), by combining the PCI, SMCI, and TCI through the constrained optimization procedure which is a new multiple remote sensing-based drought index especially using this method. Furthermore, this study attempts to determine the spatiotemporal agricultural drought patterns in a vast country (Iran) by incorporating the single drought indices, including VCI, TCI, and PCI, through principle component analysis (PCA), which has better results than other single-based indices such as NDVI, VHI, standardized vegetation index, etc., that have been used in previous research for the vast study areas. In addition, in this study, all remote sensing-based indices have been evaluated through correlation coefficient analysis with *in situ*-based meteorological indices, including the SPI and SPEI series of 1, 3, 6, 12, and 24 months which contain a long period from 2000 to 2021. Overall, this work provides a basic reference for reasonably choosing RS-based drought indexes for large-scale drought monitoring to obtain a better understanding of the environmental conditions.

II. Materials and Methods

A. Study Area

As a country in the Middle East, Iran covers an area of 1.62 million km^2. Geographically, Iran is located in West Asia and borders the Caspian Sea, Persian Gulf, and Gulf of Oman. Iran is a vast country and extends between 25° 03′ 0″ N to 39° 47′ 0″ N latitudes and 44° 05′ 0″ E to 63° 18′ 0″ E longitudes (see Fig. 1). The minimum and maximum heights of the country are −147 and 5595 m, respectively. The mean annual rainfall is about 250 mm, which means the average precipitation in Iran is less than one-third of the average rainfall in the world. The temperature range is from −36 to 60 centigrade. Iran has different types of climates, generally an arid and semi-arid country.

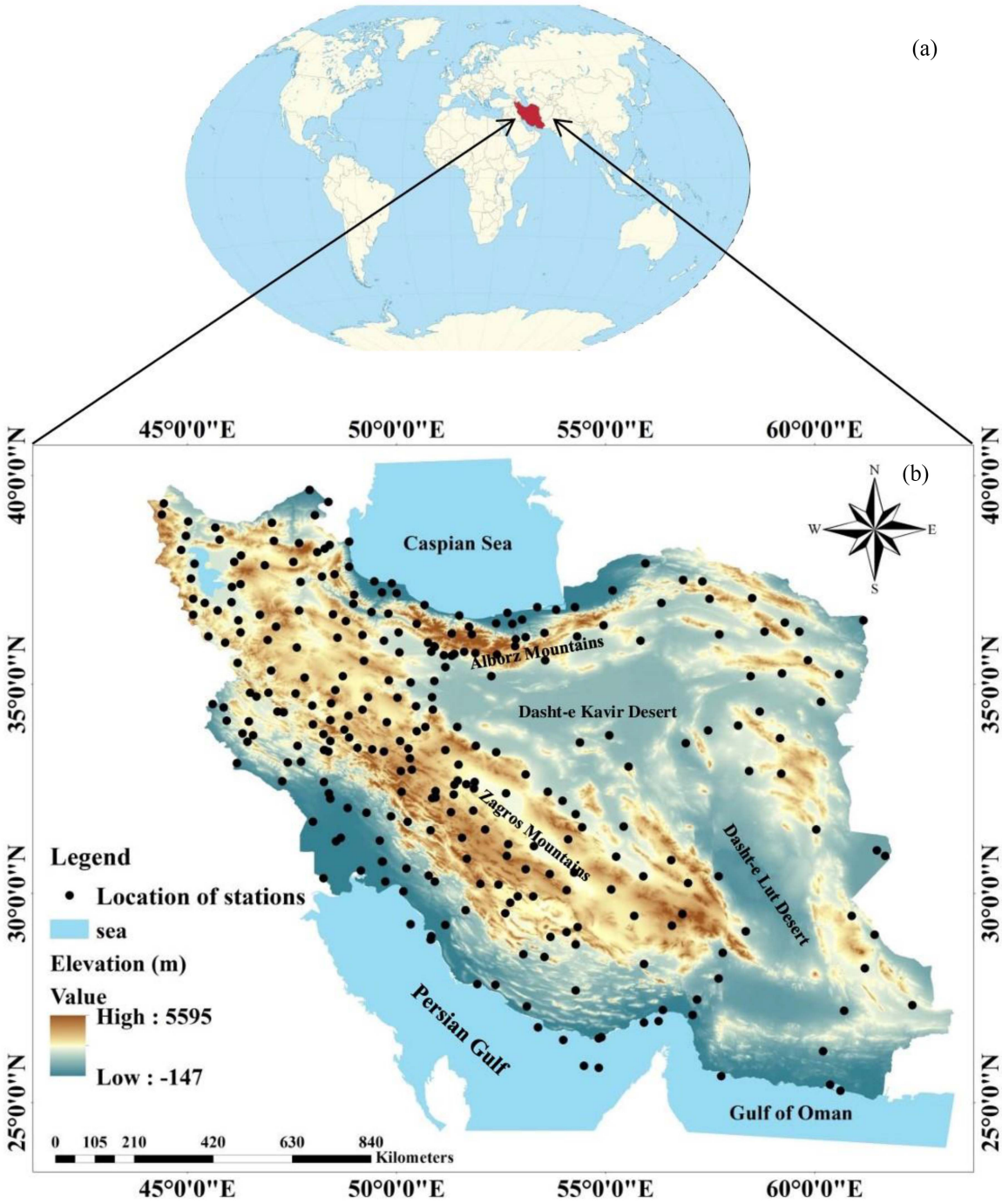

Fig. 1. (a) Location of Iran on the world map. (b) Iran map along with the distribution of meteorological stations and elevation (m).

B. Remote Sensing Datasets

Climate Hazards Group InfraRed Precipitation with Station data (CHIRPS) is a 30+ year quasi-global daily rainfall dataset [38]. CHIRPS provides 0.05° resolution satellite imagery, which compared with other precipitation datasets, including TRMM (0.25-degree spatial resolution) and Global Precipitation Measurement (0.1° spatial resolution), has a higher spatial resolution. We obtained the daily CHIRPS data through the Google Earth Engine (GEE) platform to create gridded rainfall time series and produce a precipitation condition index (PCI) for each year from 2000 to 2021. MOD11A2.061 Terra LST and Emissivity 8-Day Global 1 km product was utilized to produce the TCI for the time period 2000–2021. NDVI data were acquired from the MOD13A1 V6.1 product that presents a Vegetation Index value at a per-pixel basis with 500 m spatial resolution. The MODIS NDVI product was calculated from atmospherically corrected bidirectional surface reflectance that has been masked for water, clouds, heavy aerosols, and cloud shadows through the GEE platform during the period 2000–2021. The FLDAS

TABLE I
SATELLITE-BASED PRODUCTS INCLUDING CHIRPS DATA, LST, NDVI, AND SM

Data	Source	Data Utility	Spatial Resolution	Temporal resolution
Climate Hazards Group InfraRed Precipitation with Station data	CHIRPS packages in GEE	PCI	0.05°	Daily
MOD11A2.061 Terra Land Surface Temperature (MODIS-LST)	MODIS packages in GEE	TCI	1 km	8-Day
MOD13A1.061 Terra Vegetation Indices (MODIS-NDVI)	MODIS packages GEE	VCI	500 m	16-Day
Monthly Soil Moisture (in soil layer of 0–10 cm)	FLDAS packages in GEE	SMCI	0.1 degree	Monthly

(Famine Early Warning Systems Network (FEWS NET) Land Data Assimilation System) Noah Land Surface Model dataset with $0.1°\times\ 0.1°$ spatial resolution in the GEE platform was used to obtain monthly SM data for the years 2000–2021. Satellite-based products, including CHIRPS data, LST, NDVI, and SM have been utilized as listed in Table I.

C. Ground-Based Datasets

In this research, the monthly average precipitation, the monthly minimum, and maximum temperatures, and evapotranspiration data from 2000 to 2021 were collected from the Iran Meteorological Organization to compute the SPI and SPEI series of 1, 3, 6, 12, and 24 months for the period 2000–2021 to specify the weights of the OMDI. As well as, *in situ* meteorological indices, including the SPI and SPEI series of 1, 3, 6, 12, and 24 months were calculated in the RStudio software to verify RS drought indices and evaluate their applicability for analyzing drought conditions over large regions through the coefficient of determination between RS-based and *in situ*-based drought indexes.

D. Methodology

First, the Spatial Analyst extension has been utilized to subset the GEE datasets, which were in TIFF format to the region of interest in ArcGIS 10.7.1 software. Then, upscaling and downscaling of all images to 1 km was conducted by the nearest neighbor resampling. Afterward, drought indexes were calculated and integrated for comprehensive drought monitoring. The conventional drought indices, including VCI, TCI, PCI, SMCI, synthesized drought index (SDI), and OMDI can be classified into two types. The first one contains a single-factor index, including VCI, TCI, PCI, and SMCI, that is derived from NDVI, LST, precipitation, and SM, respectively. The second type comprises a weighted combination of multiple single-factor indices, and examples of this type are the SDI and OMDI.

In this study, the constrained optimization procedure was employed to specify the optimal weights for the MODIS-derived TCI, CHIRPS-derived PCI, and FLDAS-derived SMCI based on the SPI and SPEI to calculate the OMDI over the last two decades. The OMDI values were calculated based on the monthly scales during the period 2000–2021 to evaluate the spatiotemporal meteorological drought patterns in Iran. In addition, the spatiotemporal variability of the agricultural drought was analyzed in a Middle Eastern Country (Iran) based on the monthly scales from 2000 to 2021 through the SDI. The SDI is an agricultural drought index computed from multiple RS-based datasets, including precipitation from the CHIRPS data and LST and vegetation index from the MODIS Data. Accordingly, the temporal trends of VCI, TCI, PCI, SMCI, SDI, and OMDI on the monthly scales over the period 2000–2021 were produced. Finally, the average of all monthly maps within each year for a specific index was applied in ArcGIS to produce the spatial patterns of VCI, TCI, PCI, SMCI, SDI, and OMDI based on annual scales from 2000 to 2021. The research methodological framework is presented in Fig. 2.

1) Standardized Precipitation Index: *In situ* precipitation data is the only input parameter to compute the SPI_i over any time scale which provides early warning of drought. The SPI_i is a meteorological drought index to analyze the rainfall deficit at different timescales and assess drought conditions. Therefore, the SPI series of 1, 3, 6, 12, and 24 months are based on the probability of precipitation accumulation on a range of timescales. The SPI_i calculated in this study is based on monthly precipitation data which fits gamma distribution. Equation (1) is utilized to compute the probability density function of the gamma distribution [39]

$$\mathrm{f(x)_i} = \frac{1}{\beta^{\alpha}\Gamma\left(\alpha\right)} x^{\alpha-1} e^{\frac{-x}{\beta}} \tag{1}$$

$$\Gamma(\alpha)_{\mathrm{i}} = \int_0^{\infty} \mathrm{y}^{\alpha-1}\mathrm{e}^{-\mathrm{y}}\mathrm{dy} \tag{2}$$

where $\Gamma(\alpha)_{\mathrm{i}}$ is the gamma function as (2), i: based on the monthly scales, $\alpha_{\mathrm{i}} > 0$ and $\beta_{\mathrm{i}} > 0$: the shape and scale parameters, $\mathrm{x} > 0$: the cumulative precipitation. To fit the distribution parameters, the maximum likelihood solutions are utilized to optimally estimate α_{i} and β_i from the sample data using (3) and (4), respectively. As well as, $\bar{\mathrm{x}}$ is average rainfall and $\mathrm{A_i}$ is

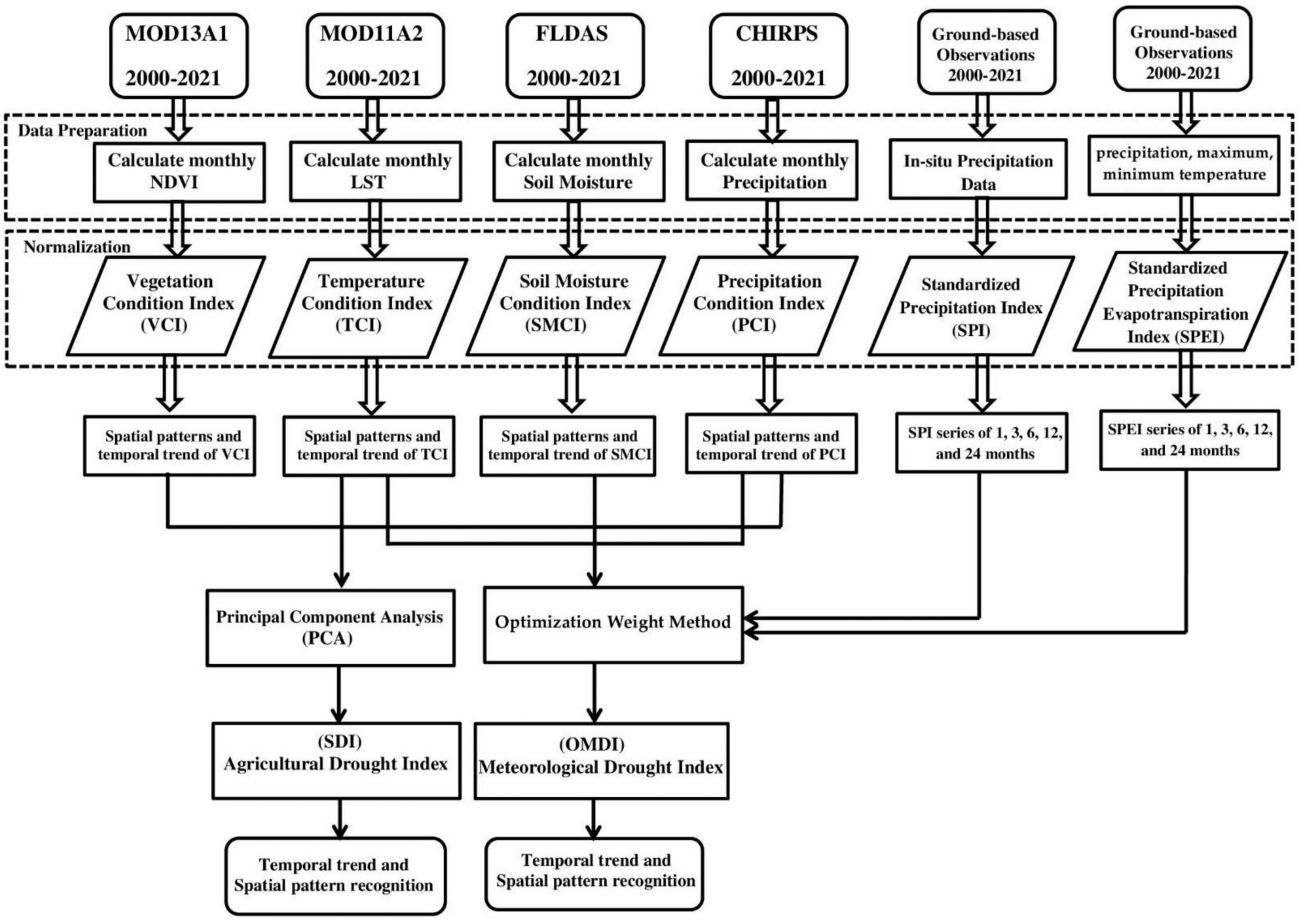

Fig. 2. Methodological framework for comprehensive drought assessment.

calculated using (5) where *n* is the number of precipitation series

$$\alpha_{\mathrm{i}} = \frac{\bar{\mathrm{x}}}{\beta} \tag{3}$$

$$\beta_{\mathrm{i}} = \frac{1}{4\mathrm{A}}\left(1+\sqrt{1+\frac{4\mathrm{A}}{3}}\right) \tag{4}$$

$$\mathrm{A_i} = \ln\left(\bar{\mathrm{x}}\right) - \mathrm{n}^{-1}\sum_{n=1}^{\infty}\left(\ln\left(\mathrm{x}\right)\right). \tag{5}$$

The cumulative probability for a given month then can be obtained by the following equation:

$$\mathrm{F(x)_i} = \int_0^x f\left(x\right)dx = \frac{1}{\beta^{\alpha}\Gamma\left(\alpha\right)}\int_0^x x^{\alpha-1}e^{\frac{-x}{\beta}}. \tag{6}$$

The SPI can be calculated as follows:

$$\mathrm{SPI}_i = \mathrm{S}\frac{\mathrm{t}-\left(\mathrm{C_1}+\mathrm{C_2t}\right)+\mathrm{C_0}}{\left[\left(\mathrm{d_3t}+\mathrm{d_2}\right)\mathrm{t}+\mathrm{d_1}\right]\mathrm{t}+1} \tag{7}$$

$$t_i = \sqrt{\ln\frac{1}{f(x)^2}} \tag{8}$$

where $\mathrm{F(x)_i}$ is Γ function, S is the positive and negative coefficient of cumulative probability distribution, when $\mathrm{G(x)} > 0.5$, $\mathrm{S} = 1$ and when $\mathrm{G(x)} \leq 0.5$, $\mathrm{S} = -1$. $\mathrm{C_0} = 2.5155$, $\mathrm{C_1} = 0.8028$, $\mathrm{C_2} = 0.0103$, $\mathrm{d_1} = 1.4327$, $\mathrm{d_2} = 0.1892$, $\mathrm{d_3} = 0.0013$ [39].

2) Standardized Precipitation Evapotranspiration Index: The computation of the SPEI_i is based on precipitation ($\mathrm{P_i}$) and potential evapotranspiration (PET_i). In this research, the PET was computed in R software which required monthly average precipitation, the monthly minimum and maximum temperatures, and latitude (Iran is located at latitude 32.5) as inputs. The SPEI_i evaluates the impact of PET on drought duration and severity which is more suitable for the detection, assessment, and observation of droughts in any climatic zone in the world. The SPEI_i applies the monthly difference between $\mathrm{P_i}$ and PET_i. Equation (9) is utilized to compute the PET_i [40]

$$\mathrm{PET}_i = 16 * \mathrm{K_i} * \left(\frac{10\mathrm{T_i}}{\mathrm{h_i}}\right)^{\mathrm{m}} \tag{9}$$

$$m_i = 6.75 * 10^{-7} * \mathrm{h_i^3} - 7.71{*}10^{-5}{*}\mathrm{h_i^2} + 1.79{*}10^{-2} \tag{10}$$

$$\mathrm{h_i} = \left(\frac{\mathrm{T_i}}{5}\right)^{1.514} \tag{11}$$

$$\mathrm{K_i} = \left(\frac{\mathrm{L_i}}{12}\right) * \left(\frac{\mathrm{N_i}}{30}\right) \tag{12}$$

where T is the average daily temperature (degrees Celsius), N and L are the number of days and the average day length of the month, h is heat index that depends on the average temperature of 12 months, α_i, β_i, and γ_i are scale, shape, and origin parameters. The m is a coefficient based on h (10). For h and k, the respective calculation formula can be defined as (11) and (12). The difference between P_i and PET_i for the month i is obtained using (13). The probability density function of a three-parameter Log-logistic distributed variable has been defined as (14). The probability distribution function of D_i based on the Log-logistic distribution is then given by (15). The SPEI_i can be computed using (16), where W = -2∗ln ($\mathrm{P_i}$), and C_0, C_1, C_2, D_1, D_2, and D_3 are constant weights [41]

$$\mathrm{D_i} = \mathrm{P_i} - \mathrm{PET}_i \tag{13}$$

$$f(x)_i = \frac{\beta}{\alpha}\left(\frac{x-\gamma}{\alpha}\right)^{\beta-1} * \left[\left(1+\left(\frac{x-\gamma}{\alpha}\right)^{\beta}\right)\right]^{-2} \tag{14}$$

$$F(x)_i = \left[\left(1+\left(\frac{\mathrm{a}}{\mathrm{x}-\gamma}\right)^{\beta}\right)\right]^{-1} \tag{15}$$

$$\mathrm{SPEI_i} = \mathrm{W} - \frac{\mathrm{C_0} + \mathrm{C_1 W} + \mathrm{C_2 W^2}}{1 + \mathrm{D_1 W} + \mathrm{D_2 W^2} + \mathrm{D_3 W^3}}. \tag{16}$$

3) Vegetation Condition Index: The VCI_i is utilized for the evaluation of vegetation in drought conditions affecting agriculture. The VCI_i compares the NDVI_i data for a given period with the highest and lowest values of the NDVI data for the whole period. Equation (17) is used to calculate the VCI_i. The NDVI_i is the smoothed 16-day NDVI_i, $\mathrm{NDVI}_{\mathrm{min}}$ and $\mathrm{NDVI}_{\mathrm{max}}$ defined as minimum and maximum values of $\mathrm{NDVI_i}$ for all pixels and periods, respectively [42], and *i* is based on the monthly scales

$$\mathrm{VCI_i} = \frac{\mathrm{NDVI_i} - \mathrm{NDVI_{min}}}{\mathrm{NDVI_{max}} - \mathrm{NDVI_{min}}} * 100. \tag{17}$$

4) Temperature Condition Index: The $\mathrm{TCI_i}$ is a RS-based thermal stress indicator to assess the water stress on vegetation due to higher soil surface temperatures. Where the $\mathrm{LST_i}$ is the smoothed 8-day land surface temperature, $\mathrm{LST}_{\mathrm{max}}$ and $\mathrm{LST}_{\mathrm{min}}$ defined as maximum and minimum LST_i value in multiyear, and *i* is based on the monthly scales. The TCI_i for each pixel and period is calculated using (18) [33], [43], [44], [45]

$$\mathrm{TCI}_i = \frac{\mathrm{LST_{max}} - \mathrm{LST}_i}{\mathrm{LST_{max}} - \mathrm{LST_{min}}} * 100. \tag{18}$$

5) Soil Moisture Condition Index: The $\mathrm{SMCI_i}$ is a normalization of SM values which ranges from 0 to 100 corresponding to alterations in SM from very dry or unfavorable status to very wet or optimum conditions. The SMCI_i for each pixel and period is calculated using (19). Where the SM_i is the soil moisture data (FLDAS) (in soil layer of 0–10 cm), $\mathrm{SM}_{\mathrm{max}}$ and $\mathrm{SM}_{\mathrm{min}}$ are the corresponding multiyear absolute maximum and minimum, and *i* is based on the monthly scales [42]

$$\mathrm{SMCI}_i = \frac{SM_i - \mathrm{SM_{min}}}{\mathrm{SM_{max}} - \mathrm{SM_{min}}} * 100. \tag{19}$$

6) Precipitation Condition Index: The PCI_i which normalized by the CHIRPS data is described for the recognition of the deficit in precipitation during a period from climate signal. Equation (20) is used to calculate the PCI_i. Where CHIRPS, $\mathrm{CHIRPS_{max}}$, and $\mathrm{CHIRPS_{min}}$ are the pixel values of rainfall, maximum and minimum of it, respectively, and *i* is based on the monthly scales. The PCI also ranges from 0 to 100 corresponding to variations in rainfall from highly unfavorable (close to 0) to optimal (close to 100) [46], [47]

$$\mathrm{PCI}_i = \frac{\mathrm{CHIRPS} - \mathrm{CHIRPS_{min}}}{\mathrm{CHIRPS_{max}} - \mathrm{CHIRPS_{min}}} * 100. \tag{20}$$

7) Synthesized Drought Index: The PCA is a dimensionality-reduction procedure that is mostly employed to reduce the dimensionality of large data sets. The SDI_i is defined as an agricultural drought indicator to monitor the spatiotemporal characteristics of agricultural drought, which is derived from weighted combinations of multiple single-factor indexes including VCI_i, TCI_i, and PCI_i. The PCA was employed in ENVI software to obtain the principal information from VCI_i, TCI_i, and PCI_i and discard the correlated signal from them. The first principal component (PCI) includes more than 75% of the uncorrelated information from the single drought indices. The SDI_i for each pixel and period is calculated using (21) [48], [49]. Therefore, in this study the SDI_i is calculated based on the monthly scales from 2000 to 2021. For instance, the average weights of the VCI_i, TCI_i, and PCI_i of SDI_i obtained as 0.22, 0.21, and 0.57 for the year 2021

$$\mathrm{SDI_i} = \alpha * \mathrm{VCI}_i + \beta * \mathrm{TCI}_i + \gamma * \mathrm{PCI}_i \tag{21}$$

where $\alpha + \beta + \gamma = 1$.

8) Optimized Meteorological Drought Index: The $\mathrm{OMDI_i}$ is defined as a multisensor microwave RS-based drought index to analyze the spatiotemporal trends of meteorological drought, which is an integration of multiple single-factor indices including TCI_i, PCI_i, and SMCI_i. This index was developed to enhance the meteorological drought observation ability of satellite remote sensing. The constrained optimization procedure is employed to specify the optimal weights (α_i and β_i) of RS-based variables; hence, multiple single-factor indices have been combined through maximizing the correlation with *in situ* drought indexes including SPI_i and SPEI_i. Overall, this procedure is utilized to integrate the TCI_i, PCI_i, and SMCI_i, using the SPI_i and SPEI_i as reference datasets [50], [51], [52], [53]. The optimization weight procedure is expressed by the following formulas:

$$\mathrm{f(x,y)_i} = \max\left(\frac{\mathrm{E}\left[(\mathrm{X} - ux) * (\mathrm{Y} - \mathrm{uy})\right]}{\sigma x * \sigma y}\right. \tag{22}$$

$$\mathrm{X_i} = \begin{cases} \mathrm{SPI}_i \\ \mathrm{SPEI}_i \end{cases} \tag{23}$$

$$\mathrm{Y}_i = \alpha_i * \mathrm{TCI}_i + \beta_i * \mathrm{PCI}_i + (1 - \alpha_\mathrm{i} - \beta_i) * \mathrm{SMCI}_i \tag{24}$$

where the constraints:

$$0 < \alpha_i < 1, 0 < \beta_i < 1. \tag{25}$$

In (22), $f(x, y)$ indicates the situation with the highest correlation between X_i and Y_i, where X_i is the SPI_i and SPEI_i,

TABLE II
DROUGHT INDICES CLASSIFICATION SCHEME FOR VCI, TCI, PCI, SMCI, SDI, AND OMDI [56]

Class Name	VCI	TCI	PCI	SMCI	SDI	OMDI
Exceptional Drought	<5	<5	<10	<5	<10	<10
Extreme Drought	5-15	5-15	10-20	5-15	10-20	10-20
Severe Drought	15-25	15-25	20-30	15-25	20-30	20-30
Moderate Drought	25-35	25-35	30-40	25-35	30-40	30-40
Mild Drought	35-40	35-40	40-50	35-40	40-50	40-50
Near Normal	40-50	40-50	50-60	40-50	50-60	50-60
No drought	>50	>50	>60	>50	>60	>60

and Y is the $\mathrm{OMDI_i}$. σx and σy are standard deviations, ux and uy are mean values of X_i and Y_i. In general, this theory has been employed to examine the correlation of the each single drought index with the SPI_i and SPEI_i of the specific month and the OMDI_i is calculated for each month from 2000 to 2021. In this study, a nonlinear programming was employed in MATLAB using Optimization Toolbox to maximize the nonlinear objective function as shown in (22) with subject to bound constraints ($0< \alpha_i < 1$, $0 < \beta_i < 1$) and obtain optimal weights of OMDI. For instance, the average optimal weights of the TCI_i, PCI_i, and SMCI_i, obtained as 0.18, 0.56, and 0.26 for the year 2021. The drought indices applied in this research were classified based on the categories used in Table II. The values of each of these indices vary from 0 to 100, where values close to 100 illustrate no drought condition and near-zero values indicate exceptional drought conditions for these indices. Hence, for meteorological and agricultural droughts monitoring, OMDI and SDI values were analyzed, and a lower value (near-zero) represents a more severe drought.

E. Data Validation

In this study, the Pearson correlation coefficient (r) has been utilized to investigate the relationships and validity of different indexes [11]. Equation (26) shows the correlation coefficients among the variables. Where "r" is a correlation coefficient that varies between -1 and 1, and n is the total number of sample sequences which is equal to 12 months of all years from 2000 to 2021 for 2500 same spatial sample points extracted from the image of each specific index in Arc GIS software. The x_i and y_i represent values of the x-variable and values of the y-variable in a sample, respectively. Then, n is the length of the datasets. $\bar{\mathrm{x}}$ and $\bar{y}$ are the average values of x_i and $\mathrm{y_i}$, respectively [54]

$$r = \frac{\sum_{i=1}^{n}(x_i - \bar{x}) * (y_i - \bar{y})}{\sqrt{\left(\sum_{i=1}^{n}(x_i - \bar{x})^2\right) * \left(\sum_{i=1}^{n}(y_i - \bar{y})^2\right)}}. \quad (26)$$

III. RESULTS AND DISCUSSION

The monthly total precipitation, the monthly minimum and maximum temperature data during the period 2000–2021 were collected at the 101 meteorological stations of Iran Meteorological Organization to calculate the SPI and SPEI series of 1, 3, 6, 12, and 24 months as shown in Fig. 3. The SPI reflects the anomalies (standard deviations from the mean) of the observed total precipitation for a certain accumulation period. When the SPI is calculated for short-term accumulation (e.g., SPI-1 to SPI-6), it can be utilized as an indicator to assess immediate effects including SM deficits and monitor agricultural drought conditions. While, the SPI is calculated for long-term accumulation (e.g., SPI-12 to SPI-48), it can be utilized to monitor streamflow, reservoir, and groundwater storage. The SPI and SPEI values more negative than -1 represent times of drought and drier periods, e.g., the SPI and SPEI values less than -2 indicate extreme drought conditions. The SPI and SPEI values between -1 and 1 illustrate near-normal condition, and the values higher than 1 represent wet conditions. For all time scales of both indices (SPI and SPEI), the main wet (2019 and 2020) periods show up in both time series. The differences between the SPI_i and SPEI_i for any time scale indicate an increase in the duration and magnitude of meteorological droughts in the SPEI series, which is associated with the temperature increase and could not be recognized using the SPI [39].

A. Spatial Patterns of Multiple Single-Factor Indices Including VCI_i, TCI_i, PCI_i, and $SMCI_i$

According to the variant ranges of vegetation indices, the intensity, affected areas, and duration of droughts can be assessed. The values of VHIs such as VCI_i and TCI_i change from 0 (an unfavorable condition) to 100 (an optimum condition), with normal conditions within 50–60 based on the average cumulative moisture and temperature conditions. Low values represent extreme moisture stress, thermal, or vegetation condition. For instance, $\mathrm{VCI}_i < 50$ represents moisture stress, $50 < \mathrm{VCI}_i < 60$ for normal moisture condition, and $\mathrm{VCI}_i > 60$ represents ideal moisture conditions [55]. As well as, drought-related stress can be evaluated according to VCI_i and TCI_i if their values are below 50. The VCI maps for the study area for the years 2008, 2019, 2020, and 2021, and the temporal trend of VCI on the monthly scales over the period 2000–2021 are shown in Fig. 4.

The higher values of VCI_i, demonstrate less drought intensity. It is observed from the VCI maps that VCI_i value in Iran is less than 40 in most areas and areas with VCI_i more than 60 are detected in the north of the country, near to the Caspian Sea. As the drought worsens, VCI_i declines and the values are less than 30 in most regions of the study area indicating intensified moisture stress from drought. Very intensive moisture stress can be noticed almost in the entire study area in 2008 and 2021. In addition, the time series of VCI during the period 2000–2021

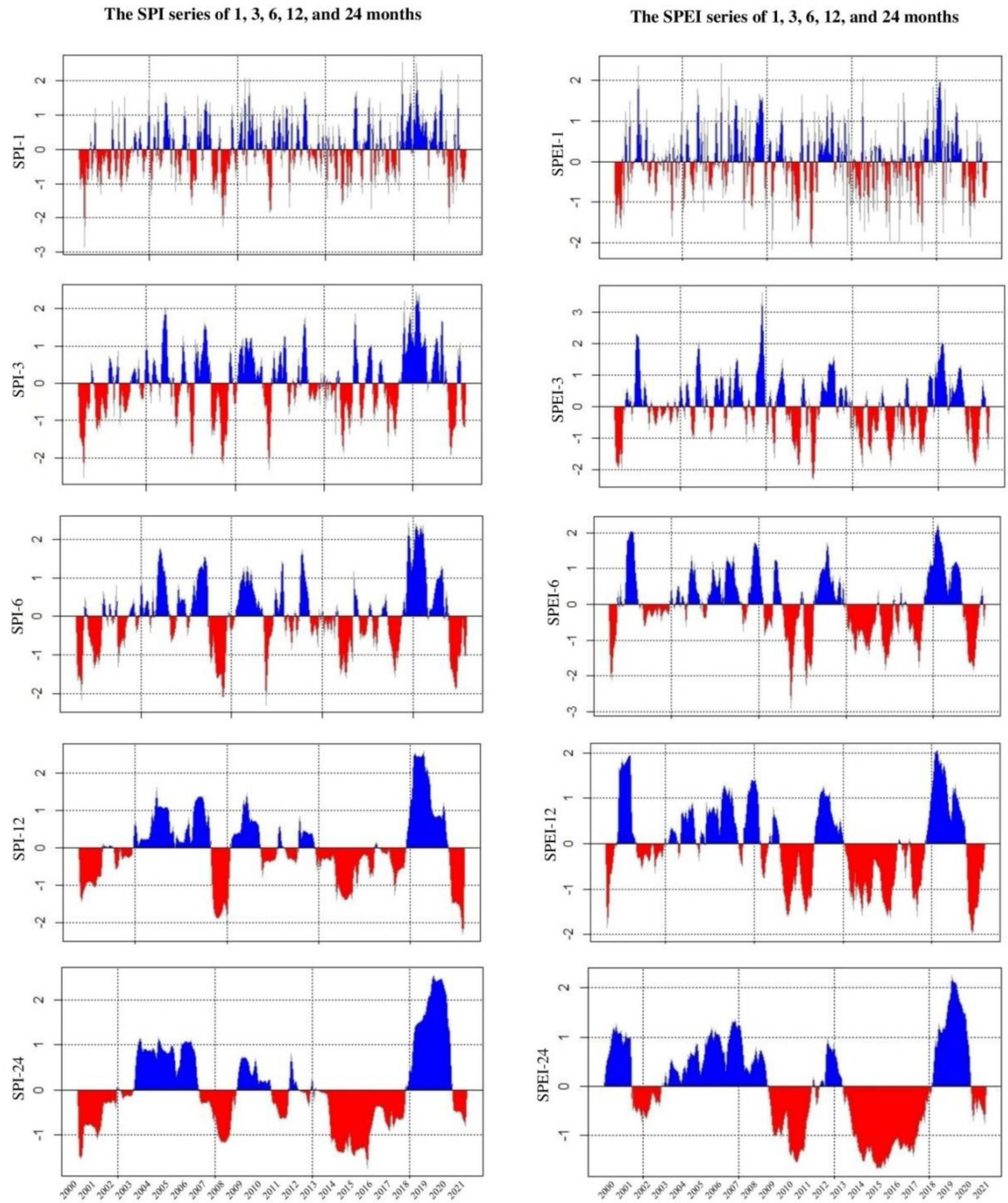

Fig. 3. Evolution of the SPI and SPEI in Iran between 2000 and 2021 for multiple timescales.

illustrates monthly values of VCI range from 21 to 36. It also demonstrates that the VCI of the year 2008 and 2021 had the highest rates of drought with the average value of 26.92 and 26.91, respectively. While the years 2019 and 2020 recorded the highest VCI values as 30.88 and 31.05, respectively, which indicate moderate drought.

The TCI is expressed in %, the TCI <5 represents exceptional drought intensity, TCI <15 represents extreme-to-exceptional drought intensity, TCI <25 represents severe-to-exceptional drought intensity, TCI <35 represents moderate-to-exceptional drought intensity, TCI <40 represents mild-to-exceptional drought intensity, $40 < \text{TCI} < 50$ indicates near normal, and TCI >50 demonstrates no drought [57]. The spatial patterns of TCI for the years 2008, 2019, 2020, and 2021, and the temporal trend of TCI on the monthly scales over the period 2000–2021 are shown in Fig. 5. The TCI analysis was performed in GEE platform and ArcGIS 10.7.1 in which higher values of TCI indicate normal conditions (located in Northern

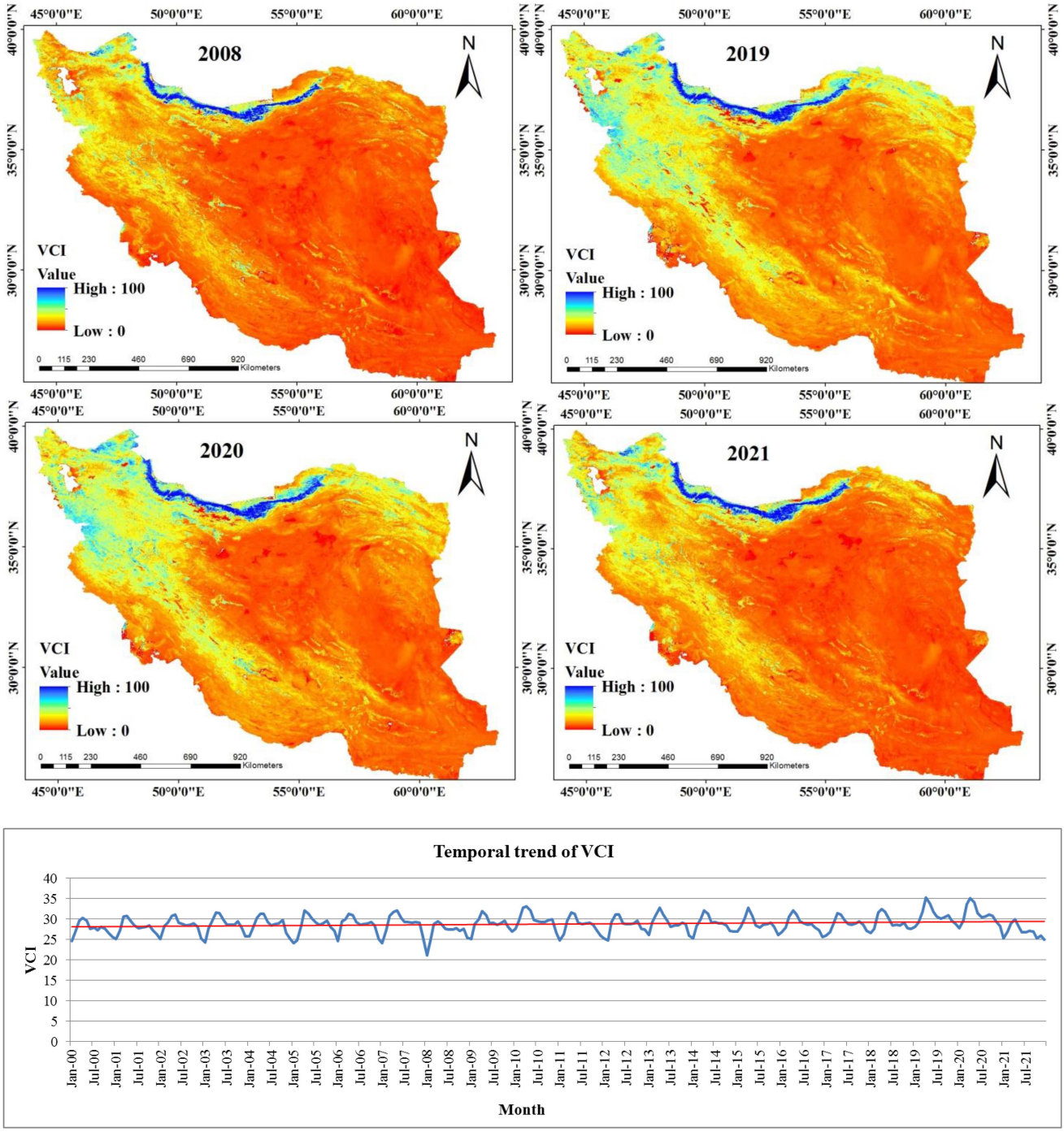

Fig. 4. Spatial patterns of VCI for the years 2008, 2019, 2020, and 2021, and the temporal trend of VCI on the monthly scales over the period 2000–2021.

Iran in regions near the Caspian Sea, northwestern parts, the Alborz Range on the north, and the Zagros Range on the west) and near-zero values indicate drought-related stress conditions [located in the central parts (deserts) and southeastern regions (Lut Desert especially Rigzar)]. Furthermore, the time series of TCI during the period 2000–2021 illustrates monthly values of TCI ranging from 27 to 47. It also demonstrates that TCI of the year 2008, 2013, and 2021 had the highest rates of drought with the average value of 32.05, 33.28, and 32.18, respectively, which indicate moderate drought. While the years 2004, 2019, and 2020 recorded the highest TCI values as 35.3, 38.27, and 36.72, respectively, which indicate mild drought.

Iran's 20-year average annual rainfall is 250 mm [58]; this statistic shows that our country's annual rainfall is much lower than the world. The average rainfall in Kerman province is 140 mm per year [59], according to the recorded statistics; this amount has decreased in recent years. In this research, the CHIRPS dataset of daily, monthly, and yearly rainfall data from 2000 to 2021 have been utilized to evaluate the spatial patterns of PCI during the period 2000–2021 within Iran as an indication

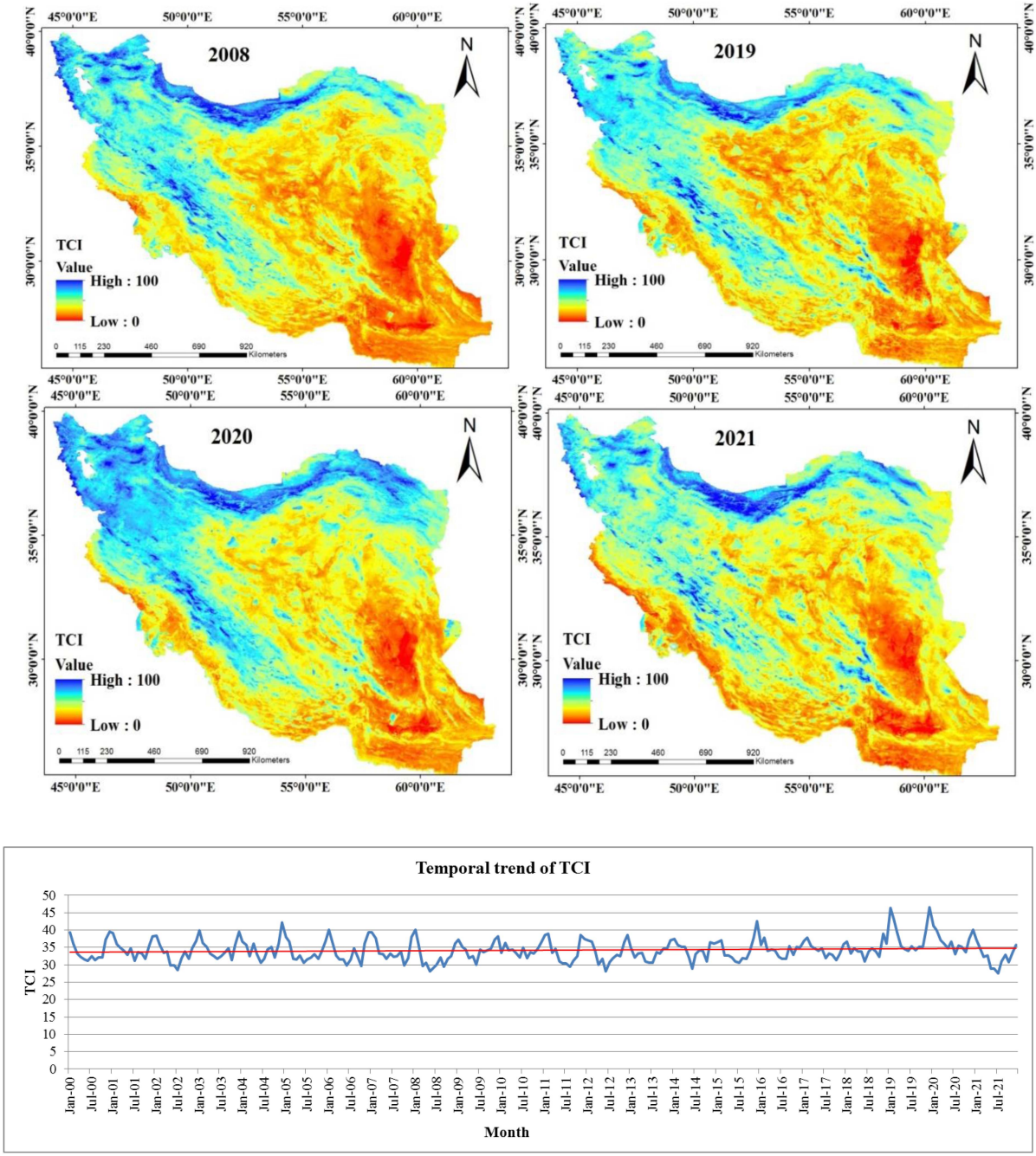

Fig. 5. Spatial patterns of TCI for the years 2008, 2019, 2020, and 2021, and the temporal trend of TCI on the monthly scales over the period 2000–2021.

of climate change. The spatial distributions of PCI for the years 2008, 2019, 2020, and 2021, and the temporal trend of PCI on the monthly scales over the period 2000–2021 are presented in Fig. 6. The PCI also varies from 0 to 100 based on variations in rainfall from highly unfavorable to optimal. According to the PCI maps in Fig. 6, more than half of the country has a low PCI value, displaying conspicuous drought conditions. Highest PCI values are recorded in Northern Iran in regions near to the Caspian Sea, representing no drought conditions. Minimum PCI values are recorded located in the central parts (deserts) and southeastern regions (Lut Desert especially Rigzar), indicating obvious drought conditions. Moreover, the time series of PCI during the period 2000–2021 illustrates monthly values of PCI range from 0.6 to 30. It also demonstrates that PCI of the year 2008 and 2021 had the highest rates of drought with the average value of 8.28 and 8, respectively, which indicate exceptional drought. While the years 2004, 2019, and 2020 recorded the highest PCI values as 12.81, 13.61, and 14, respectively, which indicate extreme drought.

SM plays an underlying role in many water-related applications, such as water resources management, drought analysis, agriculture, and climate change studies. In most regions of Iran, SM values are not measured and limited measurements do not provide sufficient spatial and temporal resolution for large

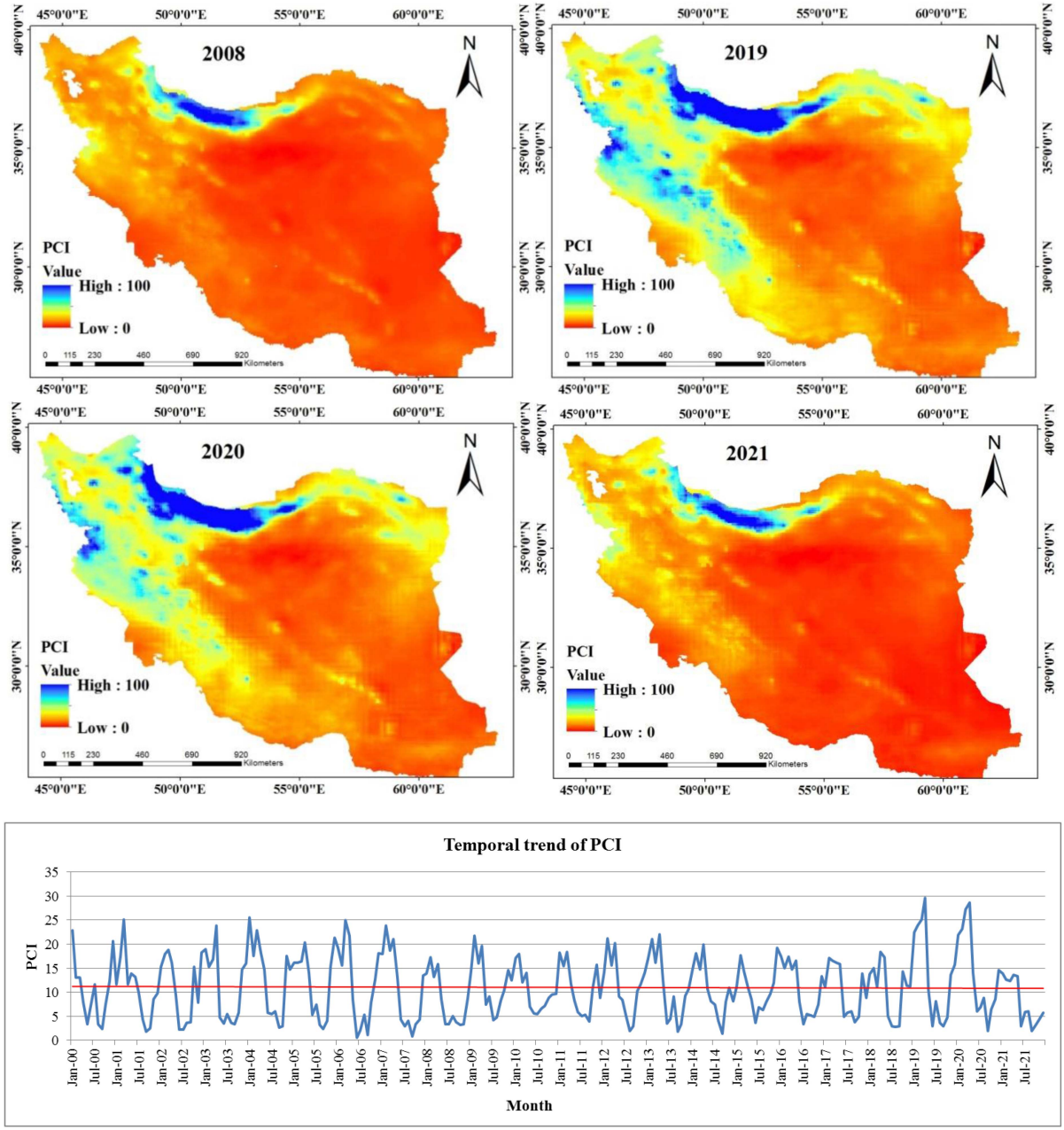

Fig. 6. Spatial patterns of PCI for the years 2008, 2019, 2020, and 2021, and the temporal trend of PCI on the monthly scales over the period 2000–2021.

study areas. Therefore, remote sensing data because of its global coverage and continuous datasets from SM can be employed to drive SM information during a long period of time in Iran. The SMCI is a SM index derived from the FLDAS datasets, which contain global monthly SM data in different depths [11]. The SM is incorporated in SMCI using a normalization considering the maximum and minimum time range values for each pixel, where values close to zero illustrate drought conditions and nearby 100 represent higher moisture conditions. The SMCI maps show spatial patterns like that of the TCI maps. The spatial patterns of SMCI for the years 2008, 2019, 2020, and 2021, and the temporal trend of SMCI on the monthly scales over the period 2000–2021 are shown in Fig. 7. According to the SMCI maps shown in Fig. 7, Northern Iran (north western and northeastern parts) in regions near to the Caspian Sea, the Alborz Range on the north, and the Zagros Range on the west exhibit no drought conditions, whereas the central parts and southeastern regions have low SMCI values, indicating very dry or unfavorable-conditions. In addition, the time series of SMCI during the period 2000–2021 illustrates monthly values of SMCI range from 19 to 62. It also demonstrates that SMCI of the year 2008, 2016, and 2021 had the highest rates of drought with the average value of 31.62, 32.87, and 30.99, respectively, which indicate moderate drought. While the years 2005, 2019, and 2020 recorded the highest SMCI values at 36.87, 38.57, and 37.52, respectively, which indicate mild drought.

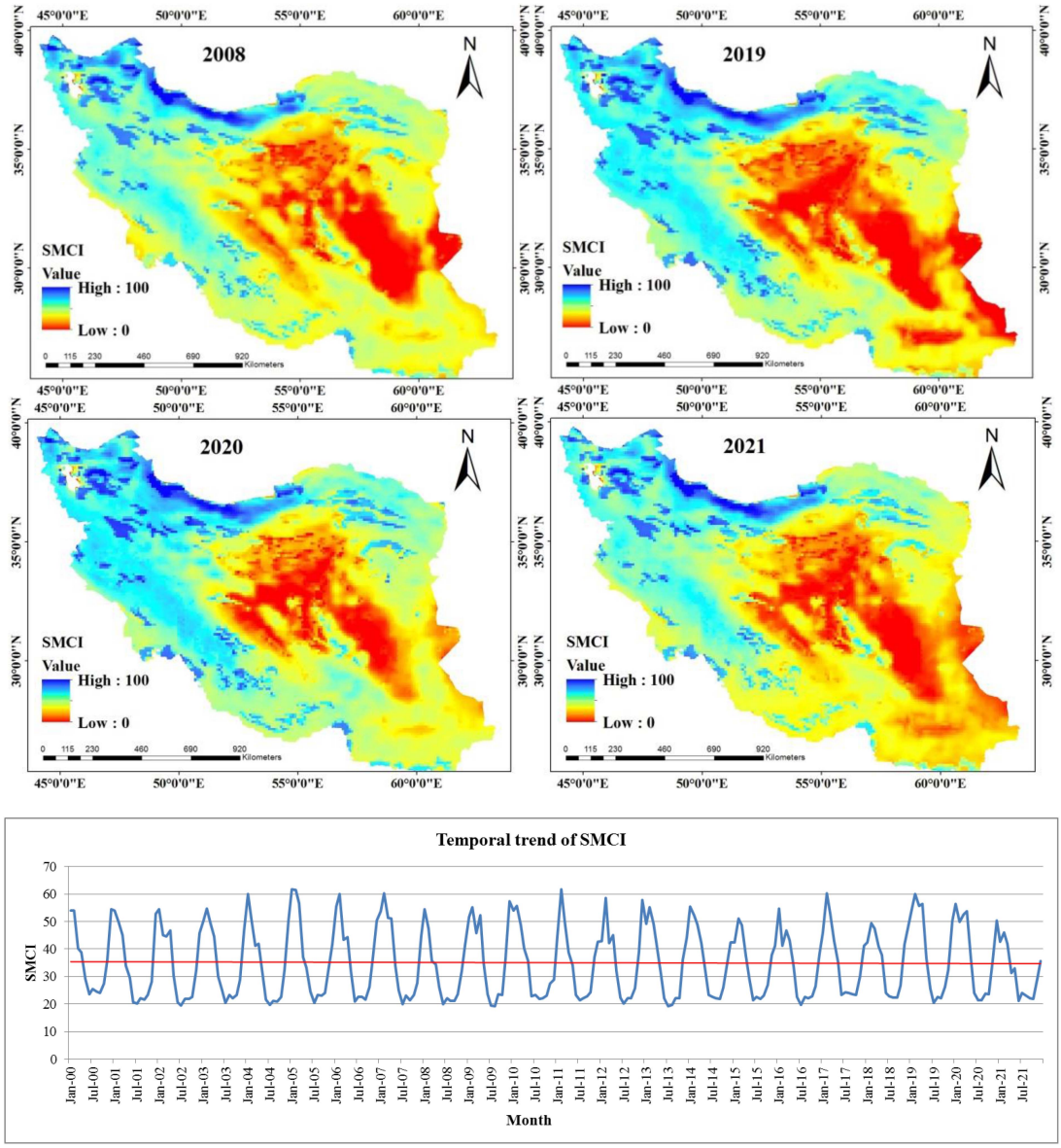

Fig. 7. Spatial patterns of SMCI for the years 2008, 2019, 2020, and 2021, and the temporal trend of SMCI on the monthly scales over the period 2000–2021.

B. Spatial Patterns and Temporal Trends of Agricultural Drought

All maps of SDI presented below have values changing from 0 to 100, where 0–10 exhibits exceptional drought, 10–20 exhibits extreme drought, 20–30 exhibits severe drought, 30–40 exhibits moderate drought, 40–50 exhibits mild drought, 50–60 exhibits near normal, and 60–100 represents no drought. Fig. 8 depicts the spatial patterns of agricultural drought over the years 2000–2021, with SDI values varying from 0 to 100. The SDI maps indicate that the SDI values mainly range from 0 to 10 (displayed by red color in the maps) during the period 2000–2021, which represents that most of the study area is under exceptional agricultural drought, while no drought area (60—100) is almost negligible.

The central parts, eastern, and southeastern regions have low SDI values (0–10), indicating exceptional agricultural drought. The Northwest of Iran, Alborz Range on the north as well as the Zagros Range on the west exhibit moderate to mild drought conditions with some green patches indicating very small drought (50–60) showing areas that may be going into or are coming out of drought. Northern Iran in regions close to the Caspian Sea have high SDI values (60–100), indicating no drought conditions (displayed by dark green color in the maps). The time series of SDI during the period 2000–2021 as shown in Fig. 9 illustrates average monthly values of SDI in Iran vary from 16 to 33. It also indicates that SDI of the year 2008 and 2021 had the highest drought rates with an average value of 19.63 and 17.24, respectively, indicating extreme drought. While the years 2019 and 2020 recorded the highest SDI values 24.79 and 24.62, respectively, which indicate severe drought. Fig. 10 demonstrates the area of agricultural drought classes on the annual scales from 2000 to 2021, based on SDI values.

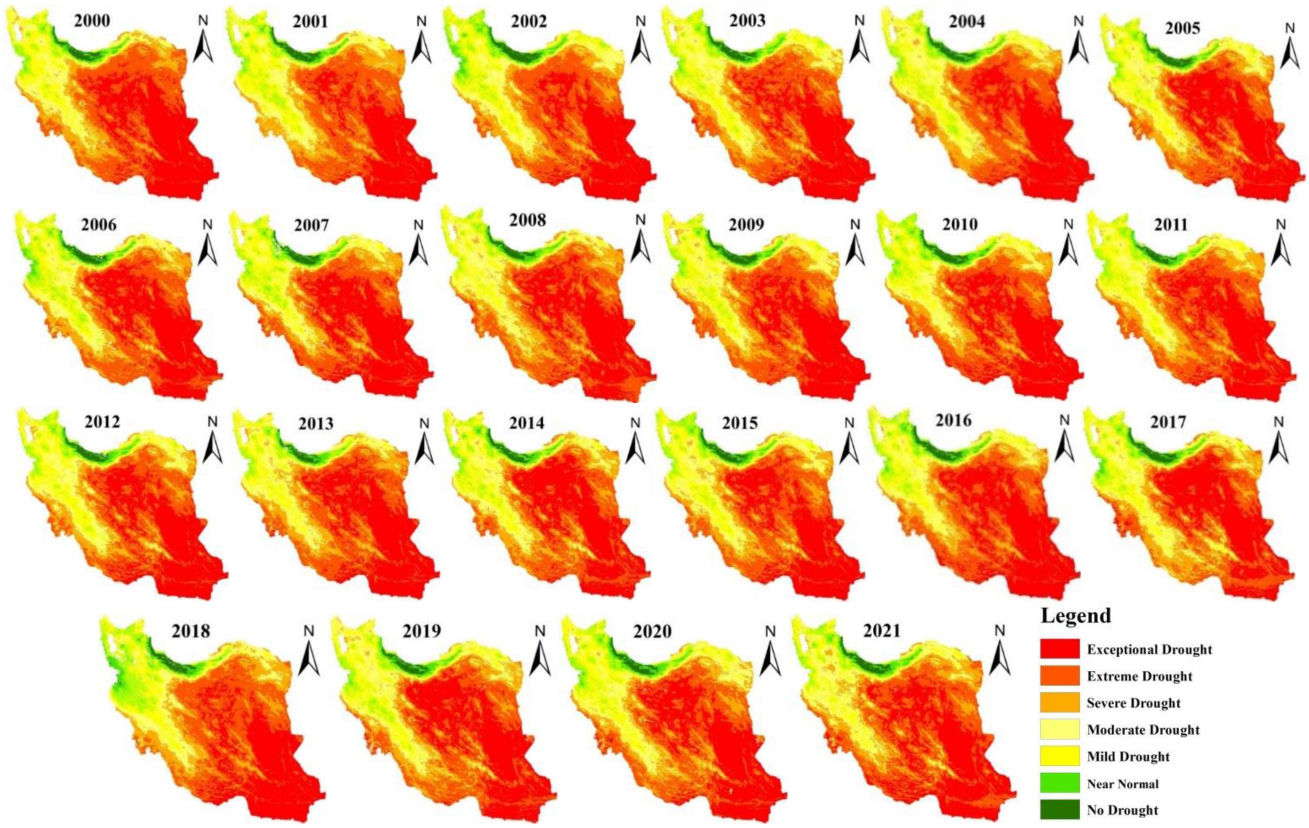

Fig. 8. Spatial patterns of agricultural drought on the annual scales over the years 2000–2021, based on SDI values.

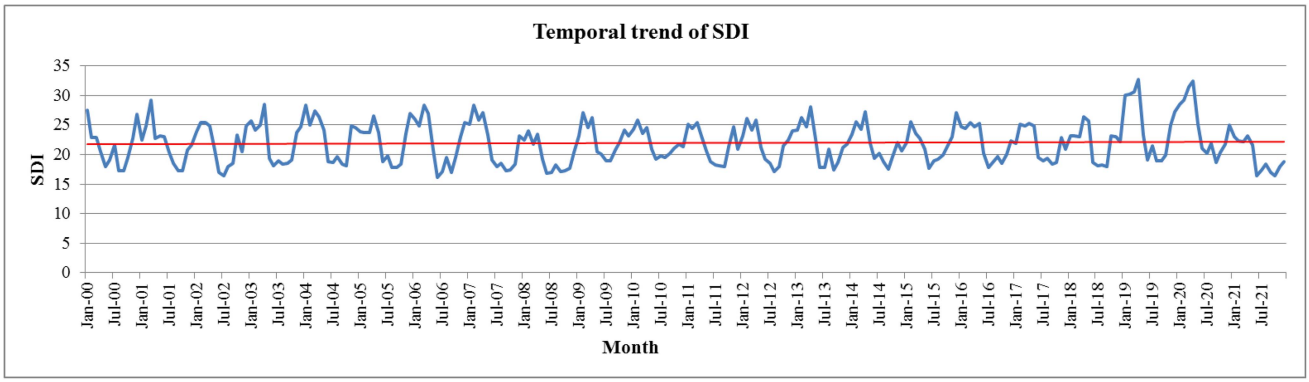

Fig. 9. Time series of agricultural drought on the monthly scales during the period 2000–2021, based on SDI values.

Most of the area of Iran prevailed in the state of drought in 2008 (36.81% exceptional drought, 28.58% extreme drought, 14.81% severe drought, 11.86% moderate drought, and 5.3% mild drought), and the intensity of drought has increased as opposed to previous years. The next year, the severity of the exceptional drought has decreased from 36.81% (593966.27 km^2) in 2008 to 30.3% of the area (489192.60 km^2) in 2009, and the area of no drought class has increased from 1.3% (21124.72 km^2) to 1.9% (30607.49 km^2). There is an analogous pattern in 2021, where almost all regions faced drought conditions (37.72% exceptional drought, 28.91% extreme drought, 14.34% severe drought, 10.99% moderate drought, and 4.6% mild drought). Near normal and no drought classes had a very limited presence (2% and 1.55%, respectively). In 2019 and 2020, most areas of Iran had higher SDI values. In the year 2019 and 2020, the severity of the drought has decreased during the period 2000–2021. The area of exceptional drought class was 29% (468005.03 km^2) in 2019 and 29% (468067.64 km^2) in 2020. The area of extreme drought class was 24.55% in 2019 and 24.15% in 2020. As well as, the area of no drought class has increased in 2019 (2.64%) and 2020 (2.54%).

According to the temporal trend of agricultural drought shown in Fig. 10, more areas were affected by exceptional agricultural drought in 2008 (36.81%) and 2021 (37.72%). As well as, the area representing extreme drought is highest in the years 2008 and 2021. Therefore, the years 2008 and 2021 have been

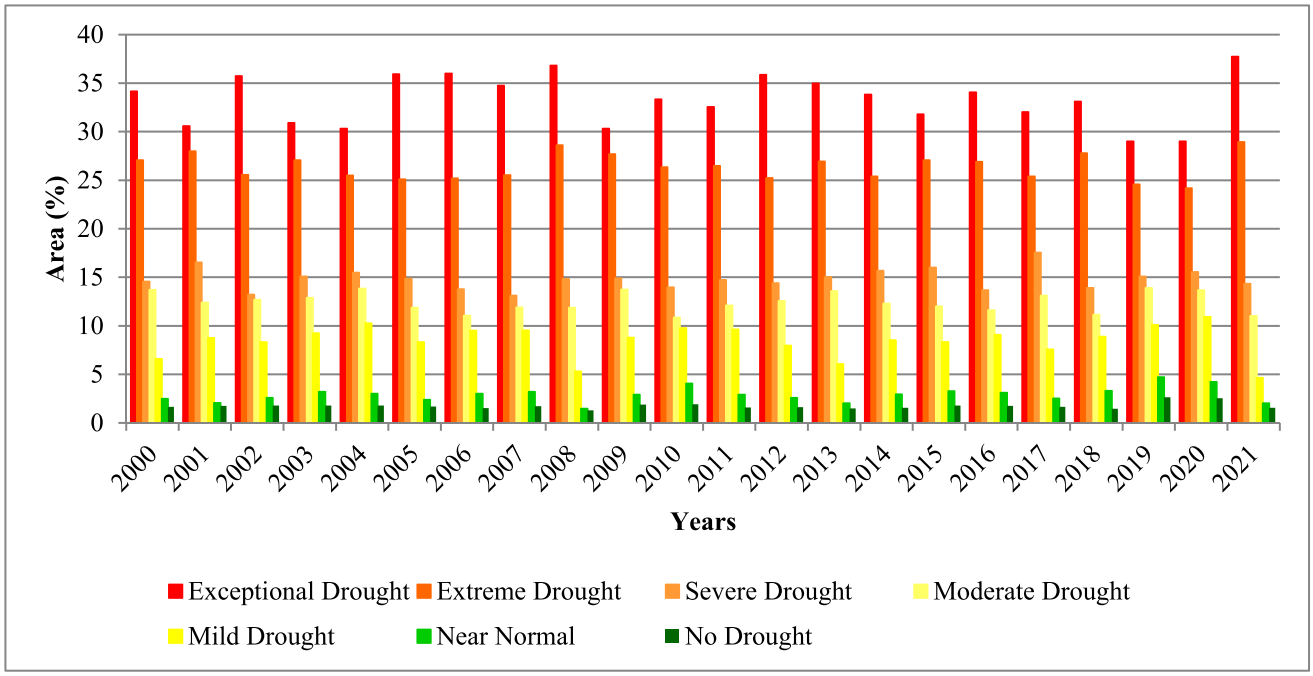

Fig. 10. Temporal trend of agricultural drought on the annual scales during the period 2000–2021, based on SDI values.

considered as agricultural drought years. The severity of the agricultural drought decreased in 2019 and 2020, and its area is lowest in 2019 and 2020 during the period 2000–2021. In addition, peak is detected in the area of no drought class in 2019, whereas the situation is the opposite in 2008.

C. Spatial Patterns and Temporal Trends of Meteorological Drought

The maps of OMDI presented below have values changing from 0 to 100, where 0–10 illustrates exceptional drought, 10–20 illustrates extreme drought, 20–30 illustrates severe drought, 30–40 illustrates moderate drought, 40–50 illustrates mild drought, 50–60 illustrates near normal, and 60–100 represents no drought. Fig. 11 depicts the spatial patterns of meteorological drought over the years 2000–2021, with OMDI values varying from 0 to 100. The OMDI maps in Fig. 11 indicate that the OMDI values mostly range from 10 to 20 (displayed by dark orange color in the maps) during the period 2000–2021, which represents that most of the study area is under extreme meteorological drought, while no drought area (60–100) is almost negligible. The time series of OMDI during the period 2000–2021 as shown in Fig. 12 illustrates monthly values of OMDI ranging from 12 to 39. It also indicates that OMDI of the year 2008 and 2021 had the highest rates of drought with the average value of 19.81 and 18.33, respectively, which indicate extreme drought. While the years 2019 and 2020 recorded the highest OMDI values as 25.78 and 25.35, respectively, which indicate severe drought. Fig. 13 illustrates the area of meteorological drought classes on the annual scales over the period 2000–2021, based on OMDI values. The central, eastern, and southeastern parts of Iran had the lowest OMDI values ranging from 0 to 10. The Northwest of Iran, Alborz Range on the north as well as the Zagros Range on the west had OMDI values ranging from 50 to 60, representing near normal condition. In 2021, most of the area of near normal class has been converted to mild drought and has decreased from 11.31% in 2020 to 5.6% in 2021.

OMDI values were lowest in 2008 and 2021, most of which were between 10 and 20, indicating extreme drought conditions. In 2008, extreme drought class dominated the area (27.56%) followed by exceptional drought (20.40%), severe drought (18.56%), moderate drought (13.56%), mild drought (12.59%), near normal (6.27%), and no drought class had a very limited presence (1.03%). There is an analogous pattern in 2021, where almost all regions faced drought conditions (27.53% extreme drought, 20.44% exceptional drought, 19.15% severe drought, 13.96% moderate drought, 12.32% mild drought, and 5.6% near normal). The area representing no drought class is lowest (1.02%) in the year 2021 during the period 2000–2021. Therefore, these years are considered as meteorological drought years in which most regions of Iran were under exceptional to extreme meteorological drought, with no drought status in some areas of Northern Iran in regions close to the Caspian Sea.

The severity of the exceptional and extreme meteorological drought decreased in 2019 and 2020. The areas of exceptional and extreme meteorological droughts are 11.72% and 20.71% in 2019, and 10.98% and 20.78% in 2020, respectively. In addition, in the year 2019 and 2020 OMDI had higher values in almost the entire Iran and no drought class had more area (3.05% in 2019 and 3.07% in 2020) compared to other years during the period 2000–2021.

The results represent that in the years 2008 and 2021 almost the entire Iran had meteorological and agricultural droughts hence these years were regarded as drought years.

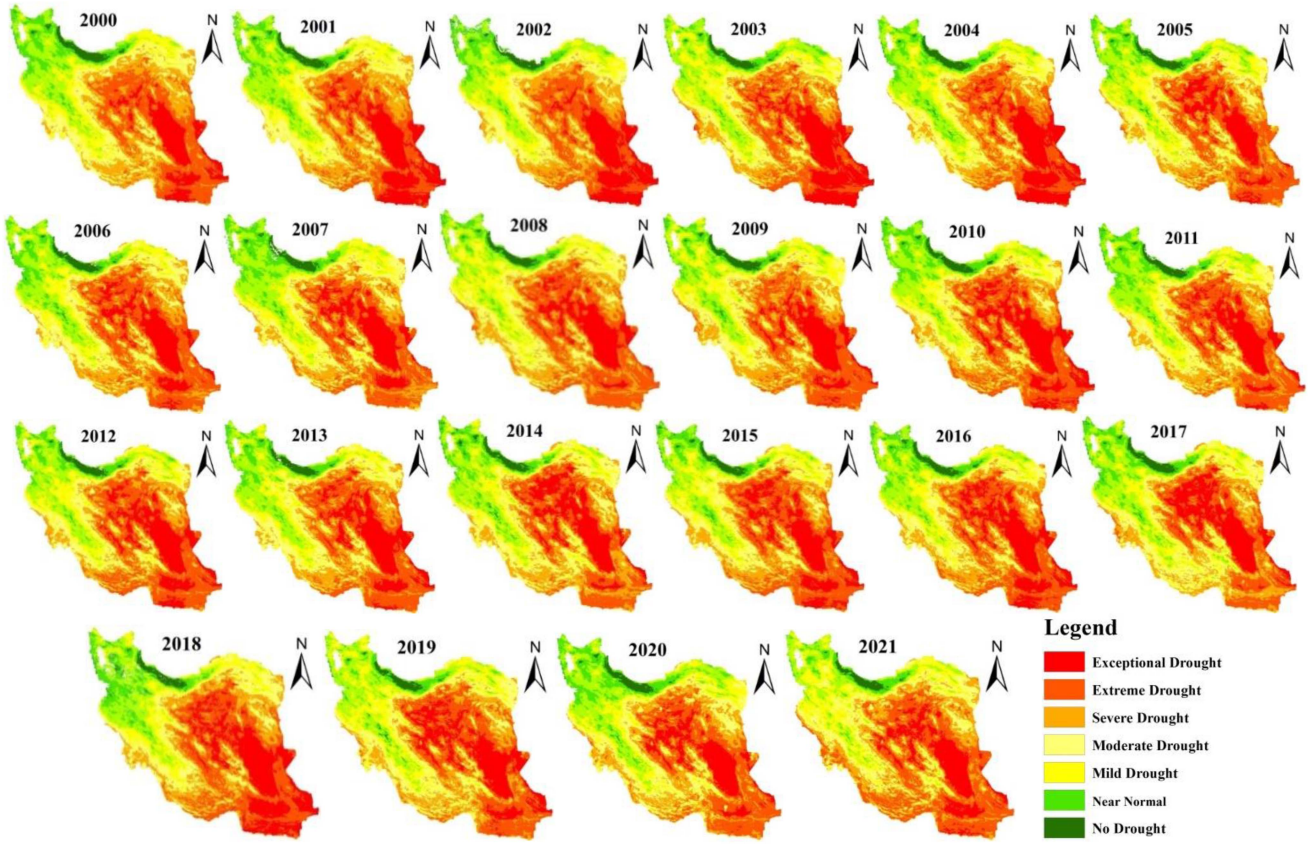

Fig. 11. Spatial patterns of meteorological drought on the annual scales over the years 2000–2021, based on OMDI values.

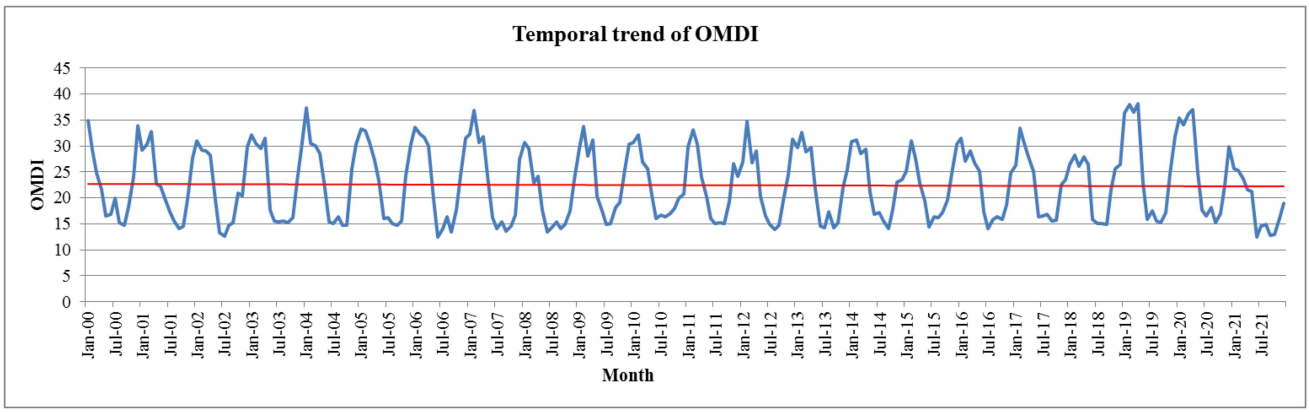

Fig. 12. Time series of meteorological drought on the monthly scales during the period 2000–2021, based on OMDI values.

The north-western side of Iran and some areas of Zagros Range were mostly having near normal meteorological drought; hence these regions are most vulnerable to drought drivers. The central, eastern, and southeastern parts of Iran were mostly having exceptional and extreme drought conditions, and the severity of meteorological and agricultural drought was also high in these areas of Iran. The cause of this severity is that rainfall in these areas is low and irregular [60], [61]. The amount of precipitation varies in different years and it may not even rain for several years. Rainfall is often heavy and in the form of showers. Due to the heat, dry air, and strong winds, the amount of evaporation and transpiration is higher than the annual rainfall in these areas [62], [63].

The meteorological drought occurs because of the rainfall deficiency and its period determines the severity of drought in a region. An agricultural drought occurs when a precipitation deficiency leads to a decrease in SM influencing pastures and rain-fed agriculture. When the rainfall is less than normal, the meteorological drought severity escalates during the time and generates more severity in the agriculture drought and affects the crop yield and native vegetation condition. Therefore, meteorological drought has a definite effect on agricultural drought,

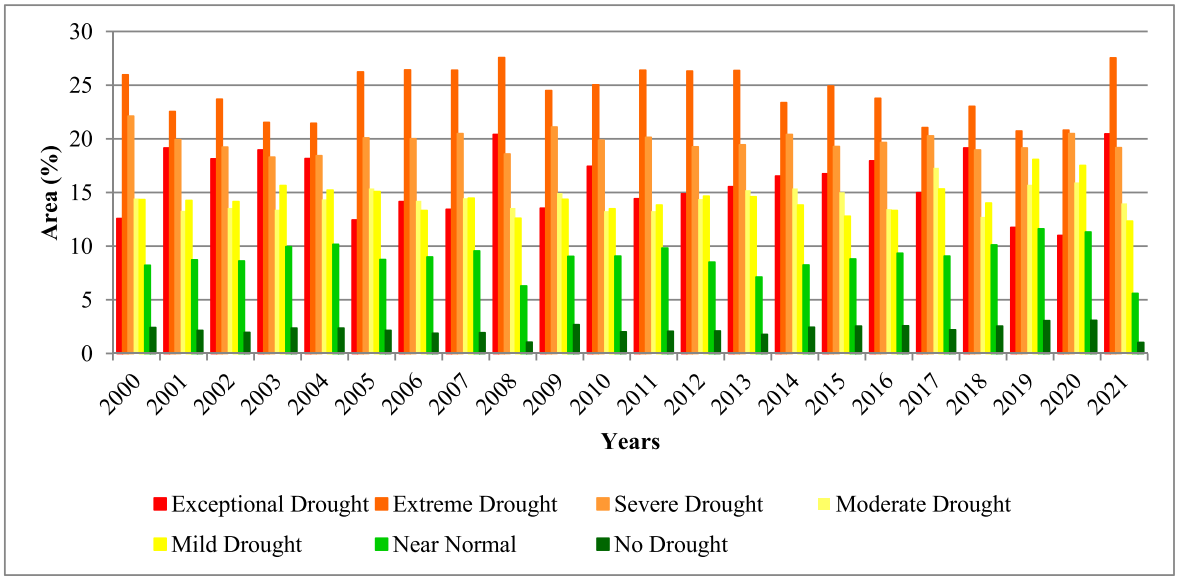

Fig. 13. Temporal trend of meteorological drought on the annual scales over the years 2000–2021, based on OMDI values.

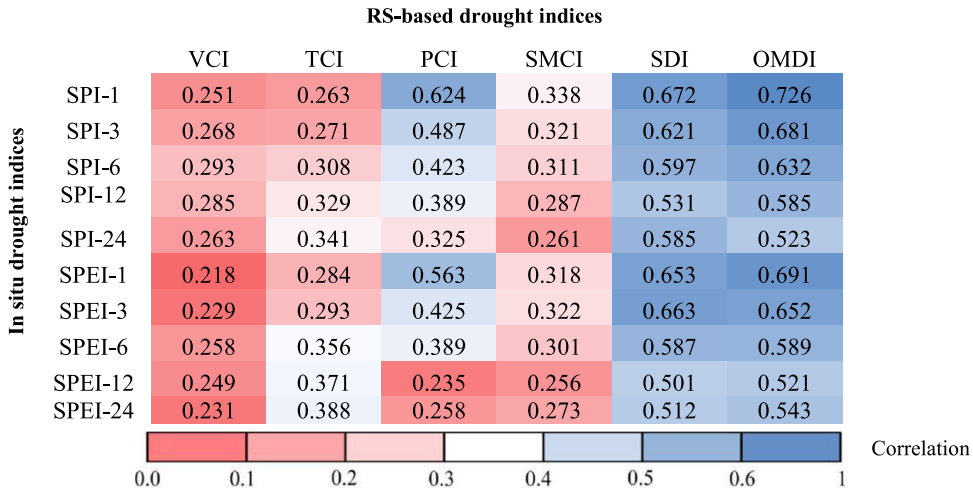

Fig. 14. Correlation coefficients between drought indices.

and the main effect is the decline of available agricultural water resources, which leads to crop water stress and reduce the yield.

The multiple RS-based drought indices are an effective tool for large-scale drought monitoring because they naturally integrate SM, vegetation information, and climate variables into drought indicators. It should be noted that this research has represented the application of combined indicators across a varying range of climate and specific environmental conditions in a large study area (1.62 million km^2). Therefore, the assessment indicated that these climatic-agricultural indices apply locally to globally.

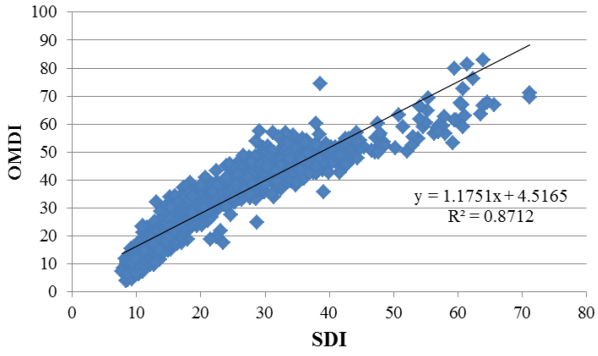

Fig. 15. Scatter correlation diagram between agricultural and meteorological droughts.

D. Correlation Analysis

The Pearson correlation coefficients (r) between RS-based drought indexes including VCI, TCI, PCI, SMCI, SDI, and OMDI, and *in situ* drought indexes are indicated in Fig. 14. In general, we included all months of all years from 2000 to 2021 for 2500 same spatial sample points extracted from the image

TABLE III
LIST OF ACRONYM

Full name	acronym	Full name	acronym
Soil Moisture Condition Index	SMCI	Optimized Meteorological Drought Index	OMDI
Precipitation Condition Index	PCI	Synthesized Drought Index	SDI
Temperature Condition Index	TCI	Standardized Precipitation Index	SPI
Vegetation Condition Index	VCI	Standardized Precipitation Evapotranspiration Index	SPEI
potential evapotranspiration	PET	Vegetation Health Index	VHI
actual evapotranspiration	ET_a	Standardized Vegetation Health Index	SVHI
Palmer Drought Severity Index	PDSI	Standardized Vegetation Index	SVI
Crop Moisture Index	CMI	Standardized Anomaly Index	SAI
Soil Moisture Drought Index	SMDI	Soil Moisture	SM

of each variable in Arc GIS software to compute the correlation coefficients between the variables. The VCI has a statistically good correlation with the SPI-6, SPI-12, SPEI-6, and SPEI-12. Overall, the correlation among the VCI and SPI series is higher than those among the VCI and SPEI series. As illustrated in Fig. 14, the TCI has a strong correlation with the long-term SPI and SPEI; therefore, the TCI is more applicable for long-term drought assessments across large areas. The results indicated that the PCI has stronger correlations with the SPI series of 1, 3, and 6 months (with average coefficients of 0.624, 0.487, and 0.423, respectively), and the SPEI series of 1 and 3 months (with average coefficients of 0.563 and 0.425). Hence, the PCI has better performance in detecting short-term drought conditions than other single drought indexes including VCI, TCI, and SMCI. The correlations among the SMCI and short-term *in situ*-based drought indices are relatively good. Accordingly, the SMCI has the potential for short-term drought analysis. Generally, single-factor drought indexes including VCI, TCI, PCI, and SMCI have specific characteristics. The PCI has the highest correlation with the SPI and SPEI series among RS-based single indices. However, the overall correlation coefficients of the combined drought indexes including OMDI and SDI within situ drought indices are higher than RS-based single indices. Among RS-based meteorological indices, the PCI and OMDI have stronger correlations with the SPI-1, as 0.624 and 0.726, respectively. The SDI has stronger correlations with the SPI series of 1, 3, and 6 months (with average coefficients of 0.672, 0.621, and 0.597, respectively) and the SPEI series of 1, 3, and 6 months (with average coefficients of 0.653, 0.663, and 0.587, respectively) than other single-factor agricultural drought indices. Fig. 14 indicates that the combined drought indexes including OMDI and SDI are highly correlated with the short-term SPI and SPEI, therefore these RS-based drought indices are more applicable to evaluate short-term drought conditions across vast areas. In addition, correlation evaluation has been utilized to evaluate the relationship between both types of droughts during the years 2000–2021 to assess the impacts of meteorological drought on agricultural drought conditions. Fig. 15 depicts the correlation coefficient among agricultural and meteorological drought. This research showed the response of agricultural drought to meteorological drought in Iran and illustrated that agricultural drought is highly linked to meteorological drought with the coefficient of determination as $R^2 = 0.8712$. Results showed that the SDI was highly correlated with OMDI because the distribution of agricultural drought intensity has a strong relationship with the meteorological droughts, which lead to a reduction of SM in Iran.

IV. CONCLUSION

In this research, the spatiotemporal variations of the agricultural and meteorological drought in Iran were analyzed using the annual series of the SDI and OMDI indices for the period 2000–2021. The OMDI is integration of multiple single-factor indices including TCI_i, PCI_i, and SMCI_i to monitor meteorological drought. The SDI is an agricultural drought index computed from multiple RS-based datasets, which includes precipitation, LST, and vegetation index. Results showed that 2008 and 2021 were the years having lowest values of OMDI and SDI illustrating extreme meteorological and agricultural drought intensity, respectively, and the area of near normal and no drought classes were the lowest in these years. The central, eastern, and southeastern parts of Iran were mostly experiencing exceptional and extreme drought conditions as the worst agricultural and meteorological drought conditions observed in the years 2008 and 2021 in the region during the last 20 years.

While, in 2019 and 2020, most areas of Iran had higher OMDI and SDI values, and the severity of drought has decreased in these years. As well as no drought area was highest in 2019 and 2020. Since there was an overall expansion in mild, near normal, and no drought classes in the year 2019 and 2020, the agricultural and meteorological drought conditions in these years were lower than in other years during the period 2000–2021. Therefore, this study concluded that 2008 and 2021 were the driest years that experienced agricultural and meteorological extreme droughts. Moreover, in this research, Pearson correlation was utilized

to consider the correlations among RS-based drought indexes and *in situ*-based drought indexes, and the overall results indicated that the correlation coefficients of the *in situ* drought indices with the combined drought indexes are higher than the RS-based single drought indexes. As well as, The PCI has the highest R with the SPI and SPEI series among RS-based single indices and can better analyze short-term drought conditions across large areas. Further, the TCI has better performance in monitoring long-term drought conditions in Iran. Nevertheless, limitations and uncertainties were presented in this research. Several future studies can be implemented in smaller study areas using Sentinel-1 SAR data and optical data from Landsat-8 or Sentinel-2 to produce the drought indices specially SM and vegetation indices. In this study, combined satellite-derived drought indices have been employed in a vast study area, which have not been well documented in previous studies. The results show specific information about choosing RS-based drought indices for monitoring meteorological and agricultural droughts across large areas. As a country in the dry belt of the earth with approximately 70% of its area in arid and semi-arid regions, droughts and floods are widespread phenomena in Iran, accordingly this work provides combined drought indices to identify drought conditions for various underlying surfaces and monitor drought processes. The detailed abbreviations and definitions used in the article are listed in Table III.

REFERENCES

[1] F. Wang et al., "Comprehensive evaluation of hydrological drought and its relationships with meteorological drought in the Yellow River basin, China," *J. Hydrol.*, vol. 584, 2020, Art. no. 124751, doi: 10.1016/j.jhydrol.2020.124751.

[2] N. Alahacoon and M. Edirisinghe, "A comprehensive assessment of remote sensing and traditional based drought monitoring indices at global and regional scale," *Geomatics, Natural Hazards Risk*, vol. 13, no. 1, pp. 762–799, Dec. 2022, doi: 10.1080/19475705.2022.2044394.

[3] A. Sharifi, "Flood mapping using relevance vector machine and SAR data: A case study from Aqqala, Iran," *J. Indian Soc. Remote Sens.*, vol. 48, no. 9, pp. 1289–1296, 2020, doi: 10.1007/s12524-020-01155-y.

[4] M. Masroor et al., "Analysing the relationship between drought and soil erosion using vegetation health index and RUSLE models in Godavari middle sub-basin, India," *Geosci. Front.*, vol. 13, no. 2, Mar. 2022, Art. no. 101312, doi: 10.1016/j.gsf.2021.101312.

[5] X. Zhao, H. Xia, B. Liu, and W. Jiao, "Spatiotemporal comparison of drought in Shaanxi-Gansu-Ningxia from 2003 to 2020 using various drought indices in Google Earth Engine," *Remote Sens.*, vol. 14, no. 7, 2022, doi: 10.3390/rs14071570.

[6] J. Zeng et al., "Improving the drought monitoring capability of VHI at the global scale via ensemble indices for various vegetation types from 2001 to 2018," *Weather Climate Extremes*, vol. 35, 2022, Art. no. 100412, doi: 10.1016/j.wace.2022.100412.

[7] S. Jalayer, A. Sharifi, D. Abbasi-Moghadam, A. Tariq, and S. Qin, "Modeling and predicting land use land cover spatiotemporal changes: A case study in chalus watershed, Iran," *IEEE J. Sel. Topics Appl. Earth Observ. Remote Sens.*, vol. 15, pp. 5496–5513, 2022, doi: 10.1109/JSTARS.2022.3189528.

[8] N. Yao et al., "National-scale variation and propagation characteristics of meteorological, agricultural, and hydrological droughts in China," *Remote Sens.*, vol. 12, no. 20, 2020, Art. no. 3407, doi: 10.3390/rs12203407.

[9] N. Alahacoon, M. Edirisinghe, and M. Ranagalage, "Satellite-based meteorological and agricultural drought monitoring for agricultural sustainability in Sri Lanka," *Sustainability*, vol. 13, no. 6, Mar. 2021, Art. no. 3427, doi: 10.3390/su13063427.

[10] A. Sharifi, J. Amini, J. T. S. Sumantyo, and R. Tateishi, "Speckle reduction of PolSAR images in forest regions using fast ICA algorithm," *J. Indian Soc. Remote Sens.*, vol. 43, no. 2, pp. 339–346, 2015, doi: 10.1007/s12524-014-0423-3.

[11] A. Sharifi, H. Mahdipour, E. Moradi, and A. Tariq, "Agricultural field extraction with deep learning algorithm and satellite imagery," *J. Indian Soc. Remote Sens.*, vol. 50, no. 2, pp. 417–423, 2022, doi: 10.1007/s12524-021-01475-7.

[12] Y. Xu, X. Zhang, Z. Hao, V. P. Singh, and F. Hao, "Characterization of agricultural drought propagation over China based on bivariate probabilistic quantification," *J. Hydrol.*, vol. 598, 2021, Art. no. 126194, doi: 10.1016/j.jhydrol.2021.126194.

[13] Q. Qin et al., "Optical and thermal remote sensing for monitoring agricultural drought," *Remote Sens.*, vol. 13, no. 24, 2021, Art. no. 5092, doi: 10.3390/rs13245092.

[14] Y. Kooch, N. Ghorbanzadeh, S. Hajimirzaaghaee, and M. Egli, "Soil functional indicators in mixed beech forests are clearly species-specific," *J. Forestry Res.*, pp. 1–7, Oct. 2022, doi: 10.1007/s11676-022-01548-4.

[15] F. A. Prodhan et al., "Deep learning for monitoring agricultural drought in south asia using remote sensing data," *Remote Sens.*, vol. 13, no. 9, 2021, Art. no. 1715, doi: 10.3390/rs13091715.

[16] S. Kitaoka et al., "Regulation of the growth of sprouting roots of black locust seedlings using root barrier panels," *J. Forestry Res.*, pp. 1–10, 2022, doi: 10.1007/s11676-022-01527-9.

[17] D. N. D. Phuong, L. M. Hai, H. M. Dung, and N. K. Loi, "Temporal trend possibilities of annual rainfall and standardized precipitation index in the central highlands, Vietnam," *Earth Syst. Environ.*, vol. 6, no. 1, pp. 69–85, 2022, doi: 10.1007/s41748-021-00211-y.

[18] Z. Wang, Y. Yang, C. Zhang, H. Guo, and Y. Hou, "Historical and future palmer drought severity index with improved hydrological modeling," *J. Hydrol.*, vol. 610, 2022, Art. no. 127941, doi: https://doi.org/10.1016/j.jhydrol.2022.127941.

[19] R. Khan, H. Gilani, N. Iqbal, and I. Shahid, "Satellite-based (2000–2015) drought hazard assessment with indices, mapping, and monitoring of Potohar plateau, Punjab, Pakistan," *Environ. Earth Sci.*, vol. 79, no. 1, pp. 1–8, 2020, doi: 10.1007/s12665-019-8751-9.

[20] S. Hasan, W. Shi, X. Zhu, S. Abbas, and H. U. A. Khan, "Future simulation of land use changes in rapidly urbanizing South China based on land change modeler and remote sensing data," *Sustainability*, vol. 12, no. 11, 2020, Art. no. 4350, doi: 10.3390/su12114350.

[21] A. Sharifi and J. Amini, "Forest biomass estimation using synthetic aperture radar polarimetric features," *J. Appl. Remote Sens.*, vol. 9, no. 1, 2015, Art. no. 097695, doi: 10.1117/1.jrs.9.097695.

[22] A. AghaKouchak et al., "Remote sensing of drought: Progress, challenges and opportunities," *Rev. Geophys.*, vol. 53, no. 2, pp. 452–480, 2015, doi: 10.1002/2014RG000456.

[23] G. Hinge, M. M. Mohamed, D. Long, and M. A. Hamouda, "Meta-analysis in using satellite precipitation products for drought monitoring: Lessons learnt and way forward," *Remote Sens.*, vol. 13, no. 21, 2021, Art. no. 4353, doi: 10.3390/rs13214353.

[24] J. Hsu, W. R. Huang, P. Y. Liu, and X. Li, "Validation of chirps precipitation estimates over Taiwan at multiple timescales," *Remote Sens.*, vol. 13, no. 2, pp. 254–272, 2021, doi: 10.3390/rs13020254.

[25] M. L. Tan, A. L. Ibrahim, Z. Duan, A. P. Cracknell, and V. Chaplot, "Evaluation of six high-resolution satellite and ground-based precipitation products over Malaysia," *Remote Sens.*, vol. 7, no. 2, pp. 1504–1528, 2015, doi: 10.3390/rs70201504.

[26] F. Pei, Y. Zhou, and Y. Xia, "Application of normalized difference vegetation index (NDVI) for the detection of extreme precipitation change," *Forests*, vol. 12, no. 5, pp. 594–610, 2021, doi: 10.3390/f12050594.

[27] V. A. Bento, C. M. Gouveia, C. C. DaCamara, R. Libonati, and I. F. Trigo, "The roles of NDVI and land surface temperature when using the vegetation health index over dry regions," *Globale Planet. Change*, vol. 190, 2020, Art. no. 103198, doi: 10.1016/j.gloplacha.2020.103198.

[28] S. Kocaaslan, N. Musaoglu, and S. Karamzadeh, "Evaluating drought events by time-frequency analysis: A case study in Aegean region of Turkey," *IEEE Access*, vol. 9, pp. 125032–125041, 2021, doi: 10.1109/ACCESS.2021.3110816.

[29] R. Jiang et al., "Assessment of vegetation growth and drought conditions using satellite-based vegetation health indices in Jing-Jin-Ji region of China," *Sci. Rep.*, vol. 11, no. 1, pp. 1–8, 2021, doi: 10.1038/s41598-021-93328-z.

[30] N. Sazib, I. Mladenova, and J. Bolten, "Leveraging the google earth engine for drought assessment using global soil moisture data," *Remote Sens.*, vol. 10, no. 8, 2018, Art. no. 1265, doi: 10.3390/rs10081265.

[31] J. Rhee, J. Im, and G. J. Carbone, "Monitoring agricultural drought for arid and humid regions using multi-sensor remote sensing data," *Remote Sens. Environ.*, vol. 114, no. 12, pp. 2875–2887, 2010, doi: 10.1016/j.rse.2010.07.005.

[32] T. V. Ha, J. Huth, F. Bachofer, and C. Kuenzer, "A review of earth observation-based drought studies in Southeast Asia," *Remote Sens.*, vol. 14, no. 15, 2022, Art. no. 3763, doi: 10.3390/rs14153763.
[33] S. Kloos, Y. Yuan, M. Castelli, and A. Menzel, "Agricultural drought detection with MODIS based vegetation health indices in Southeast Germany," *Remote Sens.*, vol. 13, no. 19, 2021, Art. no. 3907, doi: 10.3390/rs13193907.
[34] W. Jiang et al., "Impacts of drought and climatic factors on vegetation dynamics in the Yellow River Basin and Yangtze river Basin, China," *Remote Sens.*, vol. 14, no. 4, pp. 930–949, 2022, doi: 10.3390/rs14040930.
[35] A. F. Almeida-Ñauñay, M. Villeta, M. Quemada, and A. M. Tarquis, "Assessment of drought indexes on different time scales: A case in semiarid mediterranean grasslands," *Remote Sens.*, vol. 14, no. 3, pp. 565–582, 2022, doi: 10.3390/rs14030565.
[36] Z. Pei et al., "The relationship between NDVI and climate factors at different monthly time scales: A case study of grasslands in inner Mongolia, China (1982-2015)," *Sustainability*, vol. 11, no. 24, 2019, Art. no. 7243, doi: 10.3390/su11247243.
[37] Z. Wang, Z. Lu, and G. Cui, "Spatiotemporal variation of land surface temperature and vegetation in response to climate change based on NOAA-AVHRR data over China," *Sustainability*, vol. 12, no. 9, 2020, Art. no. 3601, doi: 10.3390/SU12093601.
[38] T. Dinku et al., "Validation of the CHIRPS satellite rainfall estimates over Eastern Africa," *Quart. J. Roy. Meteorol. Soc.*, vol. 144, pp. 292–312, Nov. 2018, doi: 10.1002/qj.3244.
[39] C. Liu, C. Yang, Q. Yang, and J. Wang, "Spatiotemporal drought analysis by the standardized precipitation index (SPI) and standardized precipitation evapotranspiration index (SPEI) in Sichuan Province, China," *Sci. Rep.*, vol. 11, no. 1, pp. 1–4, 2021, doi: 10.1038/s41598-020-80527-3.
[40] S. S. Wahla, J. Kazmi, A. sharifi, S. Shirazi, A. Tariq, and H. J. Smith, "Assessing spatio-temporal mapping and monitoring of climatic variability using SPEI and RF machine learning models," *Geocarto Int.*, pp. 1–22, Jun. 2022, doi: 10.1080/10106049.2022.2093411.
[41] W. Liu and L. Liu, "Analysis of dry/wet variations in the Poyang Lake basin using standardized precipitation evapotranspiration index based on two potential evapotranspiration algorithms," *Water*, vol. 11, 2019, Art. no. 1380, doi: 10.3390/w11071380.
[42] M. H. A. Baig, M. Abid, M. R. Khan, W. Jiao, M. Amin, and S. Adnan, "Assessing meteorological and agricultural drought in Chitral Kabul river basin using multiple drought indices," *Remote Sens.*, vol. 12, no. 9, 2020, Art. no. 1417, doi: 10.3390/RS12091417.
[43] E. H. Bouras et al., "Linkages between rainfed cereal production and agricultural drought through remote sensing indices and a land data assimilation system: A case study in Morocco," *Remote Sens.*, vol. 12, no. 24, 2020, Art. no. 4018, doi: 10.3390/rs12244018.
[44] E. Andujar, N. Y. Krakauer, C. Yi, and F. Kogan, "Ecosystem drought response timescales from thermal emission versus shortwave remote sensing," *Adv. Meteorol.*, vol. 2017, pp. 1–10, 2017, doi: 10.1155/2017/8434020.
[45] T. P. Singh, P. Nandimath, V. Kumbhar, S. Das, and P. Barne, "Drought risk assessment and prediction using artificial intelligence over the Southern Maharashtra state of India," *Model. Earth Syst. Environ.*, vol. 7, no. 3, pp. 2005–2013, 2021, doi: 10.1007/s40808-020-00947-y.
[46] Y. Han et al., "Monitoring droughts in the greater changbai mountains using multiple remote sensing-based drought indices," *Remote Sens.*, vol. 12, no. 3, pp. 530–547, 2020, doi: 10.3390/rs12030530.
[47] R. Khan and H. Gilani, "Global drought monitoring with big geospatial datasets using Google Earth Engine," *Environ. Sci. Pollut. Res.*, vol. 28, no. 14, pp. 17244–17264, 2021, doi: 10.1007/s11356-020-12023-0.
[48] S. Park, J. Im, D. Han, and J. Rhee, "Short-term forecasting of satellite-based drought indices using their temporal patterns and numerical model output," *Remote Sens.*, vol. 12, no. 21, 2020, Art. no. 3499, doi: 10.3390/rs12213499.
[49] Y. Cao, S. Chen, L. Wang, B. Zhu, T. Lu, and Y. Yu, "An agricultural drought index for assessing droughts using awater balance method: A case study in Jilin Province, Northeast China," *Remote Sens.*, vol. 11, no. 9, 2019, Art. no. 1066, doi: 10.3390/rs11091066.
[50] A. Zhang, G. Jia, and H. Wang, "Improving meteorological drought monitoring capability over tropical and subtropical water-limited ecosystems: Evaluation and ensemble of the microwave integrated drought index," *Environ. Res. Lett.*, vol. 14, no. 4, 2019, Art. no. 044025, doi: 10.1088/1748-9326/ab005e.
[51] A. Zhang and G. Jia, "Satellite observed reversal in trends of tropical and subtropical water availability," *Int. J. Appl. Earth Observ. Geo-Inf.*, vol. 86, 2020, Art. no. 102015, doi: 10.1016/j.jag.2019.102015.
[52] A. Zhang and G. Jia, "Monitoring meteorological drought in semiarid regions using multi-sensor microwave remote sensing data," *Remote Sens. Environ.*, vol. 134, pp. 12–23, 2013, doi: 10.1016/j.rse.2013.02.023.
[53] H. Laachrate and A. Fadil, "Assessment of drought using earth observation data and cloud computing in Morocco for 2010-2020," *Int. J. Appl. Geospatial Res.*, vol. 13, no. 1, pp. 1–20, 2022, doi: 10.4018/ijagr.298260.
[54] S. Kim et al., "Correlation analysis between hydrologic flow metrics and benthic macroinvertebrates index (BMI) in the Han River Basin, South Korea," *Sustainability*, vol. 13, no. 20, Oct. 2021, Art. no. 11477, doi: 10.3390/su132011477.
[55] W. Jiao, L. Zhang, Q. Chang, D. Fu, Y. Cen, and Q. Tong, "Evaluating an enhanced vegetation condition index (VCI) based on VIUPD for drought monitoring in the continental United States," *Remote Sens.*, vol. 8, no. 3, pp. 224–245, 2016, doi: 10.3390/rs8030224.
[56] M. Henchiri et al., "Spatio-temporal patterns of drought and impact on vegetation in North and West Africa based on multi-satellite data," *Remote Sens.*, vol. 12, no. 23, pp. 1–26, 2020, doi: 10.3390/rs12233869.
[57] V. A. Bento, I. F. Trigo, C. M. Gouveia, and C. C. DaCamara, "Contribution of land surface temperature (TCI) to vegetation health index: A comparative study using clear sky and all-weather climate data records," *Remote Sens.*, vol. 10, no. 9, 2018, Art. no. 1324, doi: 10.3390/rs10091324.
[58] M. R. Eini, M. A. Olyaei, T. Kamyab, J. Teymoori, L. Brocca, and M. Piniewski, "Evaluating three non-gauge-corrected satellite precipitation estimates by a regional gauge interpolated dataset over Iran," *J. Hydrol. Regional Stud.*, vol. 38, 2021, Art. no. 100942, doi: 10.1016/j.ejrh.2021.100942.
[59] M. Abdolahi, A. Qishlaqi, and A. Abasnejad, "Environmental hydrogeochemistry of groundwater resources in Ravar plain, Northern Kerman Province, Iran," *J. Environ. Stud.*, vol. 41, pp. 81–95, 2015.
[60] R. Modarres, A. Sarhadi, and D. H. Burn, "Changes of extreme drought and flood events in Iran," *Glob. Planet. Change*, vol. 144, pp. 67–81, 2016, doi: 10.1016/j.gloplacha.2016.07.008.
[61] H. Tabari, H. Abghari, and P. H. Talaee, "Temporal trends and spatial characteristics of drought and rainfall in arid and semiarid regions of Iran," *Hydrol. Process.*, vol. 26, no. 22, pp. 3351–3361, 2012, doi: 10.1002/hyp.8460.
[62] O. Fathizadeh, S. M. Hosseini, R. F. Keim, and A. D. Boloorani, "A seasonal evaluation of the reformulated Gash interception model for semi-arid deciduous oak forest stands," *Forest Ecol. Manage.*, vol. 409, pp. 601–613, Feb. 2018, doi: 10.1016/j.foreco.2017.11.058.
[63] V. Safarianzengir, A. Fatahi, B. Sobhani, and S. A. Doumari, "Temporal and spatial analysis and monitoring of drought (meteorology) and its impacts on environment changes in Iran," *Atmos. Sci. Lett.*, vol. 23, no. 5, 2022, Art. no. e1080, doi: 10.1002/asl.1080.

Sepideh Jalayer was born in Daregaz, Iran, in 1995. She received the M.Sc. degree in remote sensing engineering from the Shahid Rajaee Teacher Training University, Tehran, Iran, in 2022.

Her research interests include geomatics, satellite image processing, and land use/land cover mapping.

Alireza Sharifi was born in Tehran, Iran, in 1981. He received the M.Sc. and Ph.D. degrees in remote sensing engineering from the University of Tehran, Tehran, Iran, in 2008 and 2015, respectively.

He is currently an Associate Professor of remote sensing with the Faculty of Civil Engineering, the Shahid Rajaee Teacher Training University, Tehran, Iran. He focused on Earth Observation Programs, for the development of precision agriculture, forestry, hydrology, flood mapping and also environmental monitoring with the help of satellite imagery. In particular, he is involved in GEOAI program for Food Security and Environmental Monitoring.

Dariush Abbasi-Moghadam received the B.S. degree from the Shahid Bahonar University, Kerman, Iran, in 1998, and the M.S. and Ph.D. degrees from the Iran University of Science and Technology, Tehran, Iran, in 2001 and 2011, respectively, all in electrical engineering.

He was primary with the Advanced Electronic Research Center—Iran from 2001to 2003 and worked on the design and analysis of satellite communication systems. In September 2004, he joined Iranian Telecommunications Company, Tehran, as a Research Engineer. He is currently with the Department of Electrical Engineering, Shahid Bahonar University of Kerman, Kerman, Iran, as an Associate Professor. His research interests include the area of wireless communications, satellite communication systems, remote sensing, and signal processing.

Aqil Tariq received the Ph.D. degree in photogrammetry and remote sensing from the State Key Laboratory of Information Engineering in Surveying, Mapping, and Remote Sensing, Wuhan University, Wuhan, China, in 2021.

He is currently working with the Department of Wildlife, Fisheries, and Aquaculture, Mississippi State University, Starkville, MS, USA. His research interests include photogrammetry, 3-D geoinformation, urban analytics, spatial analysis to examine land use/land cover, geospatial data science, agriculture monitoring, natural hazards (forest fire, landslide, droughts, flood) forest monitoring, forest cover dynamics, spatial statistics, multicriteria algorithms, ecosystem sustainability, hazards risk reduction, statistical analysis and modeling using Python, R, and MATLAB.

Shujing Qin currently works with the State Key Laboratory of Water Resources and Hydropower Engineering Science, Wuhan University, Wuhan, China. Her research interests include flux measurement and modeling of terrestrial ecosystem, eco-hydrology, land-atmosphere interaction, and climate change.